CARBON DIOXIDE CAPTURE BY COMPUTATIONALLY DESIGNED SELF-ASSEMBLED AMYLOID BIOMATERIALS

A Thesis

by

YEONSU KWAK

Submitted to the Office of Graduate and Professional Studies of
Texas A&M University
in partial fulfillment of the requirements for the degree of

MASTER OF SCIENCE

Chair of Committee, Hae-Kwon Jeong
Co-Chair of Committee, Phanourios Tamamis
Committee Member, Raymundo Arroyave

Intercollegiate Faculty Chair, Efstratios Pistikopoulos

August 2017

Major Subject: Energy

ABSTRACT

Various materials capturing CO_2 have been developed for addressing the threat of climate change. Recently, physical adsorbents are proposed as strong alternatives for conventional chemical absorbents with high regeneration energy; however, the former usually has an issue of low stability especially in humid condition. Herein, it is shown that amyloid biomaterials from novel computational design are effectual for CO_2 capture. After the computational design and validation using in-house protocol to capture multiple CO_2 molecules per peptide, self-assembling amyloid biomaterials are fabricated from promising peptides. Breakthrough measurement articulates that the biomaterials can selectively capture carbon dioxide over nitrogen. Unit CO_2 uptake demonstrates that computational approach on the mechanism of CO_2 capture is compatible with experimental result. 100℃ is sufficient temperature to regenerate the biomaterials, where the additional vacuum swing can be supportive. Computational secondary structural analysis verifies that designed peptides inherently retain stable structure rich in β-sheets. All the results show that proposed biomaterials are strong alternative, and the novel computational method can be the new criterion for CO_2 adsorbent design.

ACKNOWLEDGEMENTS

I would like to thank my committee chair, Dr. Hae-Kwon Jeong, and my committee co-chair, Dr. Phanourios Tamamis, for their advice and genuine support throughout the course of this research. Dr. Jeong showed me know how to think critically and solve a problem with a mindset of an engineer. Dr. Tamamis helped me understand true professionalism and enthusiasm as a researcher. Thanks also go to my committee member, Dr. Raymundo Arroyave for his approval to join in and his guidance. Many of the ideas for drawing an entire perspective of this research come from the distinguished lectures of Dr. Benjamin Wilhite, Dr. Nimir Elbashir, and Dr. Faraque Hasan. Throughout the research, I was helped by Sai Vamshi Reddy Jonnalagadda and Moonjoo Lee, and I wanted to thank them as their dedication inspired me.

Thanks also go to my Korean friends in Energy Institute: Alim Kim, Chang-kyu Kim, Michael Sungyeol Bae, Jinhyeun Kim, and Joonjae Ryu for being close friends here. Thank all of my foreign friends in Energy Institute: Ahmed, Almostafa, Asha, Frank-Eric, Iordanis, John-Kennedy, Jorge, Karthik, Mohamad, Mohamad-Osman, Samuel, Shayan, Tarek, Vipasha, and William for making me feel comfortable. I really appreciate the help by research group colleagues during hard times: Moonjoo Lee, Sai Vamshi Reddy Jonnalagadda, Asuka Orr, Chang-hyun Choi, Chrysoula Kokotidou, Zingze Sun, Febrian Hillman, Mohamad Rezi Abdul Hamid, and Yuchen Hsu. Thank you to the department faculty: Dr. Efstratios Pistikopoulos, and the academic program coordinator: Dr. Valentini Agathi Pappa, and associate director: Mr. Jeff Sammons for always being on my side. Financial and administrative support from EDRC of Seoul National University through the master course is highly appreciated, especially from Ms. Daeun Hwang, Ms. Yisol Kim, Dr. Jaehyun Cho, Dr. Chonghun Han, and Dr. Jongmin Lee. Last but not least, special thanks to dear my friends, and my little sister, little brother, mother and father for their lovely encouragement.

CONTRIBUTORS AND FUNDING SOURCES

Contributors

This work was supervised by a thesis committee consisting of Professor Hae-Kwon Jeong and Professor Phanourios Tamamis of Texas A&M Energy Institute & Artie Mcferrin Department of Chemical Engineering, and Professor Raymundo Arroyave of the Department of Material Engineering.

All work for the thesis was completed by the student, under the advisement of Sai Vamshi Reddy Jonnalagadda and Moonjoo Lee in the Artie Mcferrin Department of Chemical Engineering at Texas A&M University. Breakthrough system setup was conducted in part by Moonjoo Lee in the Jeong's lab of the Artie Mcferrin Department of Chemical Engineering at Texas A&M University. The fabrication of amyloid biomaterial is guided by Chrysa Kokotidou of the Department of Chemistry at Crete University. The methodology of computational design of functional self-assembling peptides is based on the work of Sai Vamshi Reddy Jonnalagadda, Chang-Hyun Choi, and Asuka Orr in Tamamis lab of the Artie Mcferrin Department of Chemical Engineering at Texas A&M University.

Funding Sources

Graduate study was supported by a fellowship from Texas A&M Energy Institute and a full-funding research scholarship from EDRC (Engineering Development Research Center) of Seoul National University. This work was made possible by the research grant of Professor Hae-Kwon Jeong and Professor Phanourios Tamamis.

TABLE OF CONTENTS

LIST OF FIGURES

LIST OF TABLES

NOMENCLATURE

CCUS	CO2 Capture, Utilization, and Sequestration
CCS	CO2 Capture and Sequestration
GAITIG	Glycine-Alanine-Isoleucine-Threonine-Isoleucine-Glycine
GAIIG	Glycine-Alanine-Isoleucine-Isoleucine-Glycine
MD	Molecular Dynamics
MOF	Metal-Organic Framework
MEA	Monoethanolamine
REMD	Replica Exchange Molecular Dynamics (Simulations)
ZIF	Zeolite-Immidazole Framework
n_{ads}	The Number of Moles Adsorbed on the Adsorbent
V_{CO2}	Volume of CO_2 adsorbed
$V_{CO2,EV}$	Volume of CO_2 adsorbed at Empty Volume
P_{atm}	Standard Pressure
P_{EV}	Pressure at Empty Volume
y_f	The Mole Fraction of CO_2 in the Feed (CO_2/N_2)
Q_f	The Volumetric Flow Rate of the Feed (CO_2/N_2)
t_t	Dynamic Delay Time of Regenerated Sample $= \int_0^\infty (1 - \frac{C}{C_0})\, dt$
T_b	Bed Temperature
ε_T	Bed Porosity
C_{CO_2}	Dynamic Composition of CO_2
τ	Delay Time Due to Adsorption
C_{actual}	Actual Capacity of the Adsorbent
$C_{1:1}$	The Capacity of the Amyloid Biomaterial with 1:1 Binding Ratio (Peptide and CO_2)
N_{CO_2}	The number of CO_2 Molecules captured per strand

1. INTRODUCTION

1.1 Addressing Climate Change

Recent energy infrastructure and industry mostly rely upon the utilization of fossil fuels.[1] Oxidizing such fuels via combustion gives rise to a huge amount of anthropogenic CO_2 emission. CO_2 has mainly affected greenhouse effect, which causes diverse problems including current sea-level rise from the meltdown of pole glaciers and brings abnormal climate changes.[2] The effect is due to the molecular vibration of CO_2, which absorbs and re-emits photon energy in the wavelength region of infrared radiation from sunlight.[3] The instantaneous forcing of CO_2 in terms of greenhouse warming is relatively low. The cumulative forcing of CO_2, however, is hardly negligible due to its great portion in the atmosphere.[3] The industrial revolution has made a significant difference in the air composition. Over the last five decades, the CO_2 fraction in air shows an increment of $0.25 \pm 0.21\%$ per year.[4] Earth's surface has been warmed roughly 0.8℃ in the past 100 years.[5] The sum of the main sources of CO_2 that contributes to the greenhouse effect is in the following equation.[6] This indicates that the system using high-energy source including coal, natural gas, and oil should be primarily mitigated.

$$F = F_{Solid} + F_{Liquid} + F_{Gas} + F_{Flare} + F_{Cement} + F_{nonfuelFC} + F_{Bunkers}$$

(~35%) (~36%) (~20%) (<1%) (3%) (<1%) (4%)

Various methodologies have been suggested to deal with ongoing threats of climate changes. Developing alternative energy with low CO_2 emission is based on renewable energy[7], inherently energy-efficient or conservative process[8], and the prevention of direct emission of CO_2 into an atmosphere[9] and the like. Alternative energy is promising but still far from commercialization. It has been shown that the utilization of alternative energy is useful for small-scale industry, but is not sufficiently for the large-scale industry.[7] The novel design process for energy conservation is

required but cannot be a conclusive solution since the CO_2 emission over a certain amount is inevitable. The latter referred to as CCUS has been regarded as one of the most feasible solutions to address climate changes due to CO_2 increase in the air.[10] It mainly captures CO_2 from huge anthropogenic sources, compresses, and transports it to the plant for CO_2 utilization or specific geological storages for safe sequestration. This systematic approach offers a mid-term solution for existent power plants using petroleum and natural gas.[10] With the advantage of the economies of scale, it could be more applicable to large anthropogenic CO_2 sources. The U.S. Department of Energy has a plan to develop large-scale CCS project in 2018.[11] In line with enhanced oil recovery[12] and shale gas revolution[13], chances are fossil fuel industry will linger over several decades forward, which implies that CCUS would remain important.

CO_2 capture technology can mitigate the detrimental effect of direct emission of CO_2 from the power plant to the atmosphere. CO_2 capture is most effective when it is applied to high concentration (<20%) flue gasses from power plants.[14] Especially at the coal-based power plant, around 15% of CO_2 emission from flue gas is exemplary.[15] Various methods for CO_2 capture in the plant have been investigated; there are most representatively Post and Pre-combustion, and Oxy-fuel combustion technology. No one is distinctively best; a technology can be selected for specific needs and requirements. To apply technology for ongoing power plants, post-combustion technology and oxy-fuel combustion technology are of critical importance for the reduction of flue gas.[14] This is because CO_2 capture plant, referred to as a stripper, can be additionally installed beside the previously installed power plant. Sorbents in strippers are vital to capturing CO_2 over impurities. The selectivity helps lower the impurities in CO_2 stream for the decent operation in the following procedure.[16] CO_2 needs to be very pure because an even low humidity can lead to a fracture or rupture due to the ice or carbohydrate formed during the transportation.[17] In addition, material regeneration in a stable manner is a prerequisite for selecting good sorbents. [18] In other words, CO_2 needs to be easily detachable from sorbents by heating, and in such a process, sorbents should not be damaged. The current CO_2 sorbents are discussed in the next section.

1.2 Current CO_2 Sorbents

To capture CO_2 in the post-combustion process, chemical or physical agents with a variety of material types have been developed.[10, 19] The design and specific configuration of capture plant are different for each type of sorbents. The objective of each type of sorbents is also different for the purpose of specific sweetening plants. To achieve both the lowest cost and the highest efficiency, promising candidates have been developed. Recently, with the emergence of nanotechnology, an approach from microstructural synthesis and modification has been widely favored to elaborate complicated nanomolecules as CO_2 sorbent.[18]

Adsorbents and absorbents are worth being distinguished in terms of their capturing mechanisms. The adsorbent attracts the molecule of a substance by its surface. For the sake of large amount of adsorption, the large surface area would be the primary factor that affects the capacity in a positive way.[20] The absorbent, however, is distinguishable as it attracts the molecule by its bulk, not by its surface. In the interest of the practical application of chemical absorption, gas-to-liquid mass and heat transfer between the absorbent and target molecule would be deterministic.[20] Here, adsorbents are mainly studied to obtain a deeper understanding of its mechanism.

Chemical adsorbents comprise amine-based, potassium or lithium-based, magnesium or calcium-based materials, etc. They react to CO_2 with a large heat, forming carbamate or other derivatives. In general, Alkaloamine including MEA, DEA, and MDEA have been widely used for CO_2 capture in the power plant.[10] Zwitterion mechanism explains the reaction of primary or secondary amine with CO_2, which is reviewed in the Chapter II.[21] In the presence of water, the sterically hindered primary or secondary amine can formulate bicarbonate.[19] The amines can be alternatively utilized for the impregnation into silica supports or covalently tethered oxide supports. From this technique, various microporous and mesoporous solid materials supported with amine functionality have been developed to chemisorb CO_2 from flue gas, which involves activated carbon, polymer-based sorbents, silica-supported sorbents, alumina-supported

sorbent, and so on.[22] Covalently tethered amine sorbents have an advantage that can be regenerated under the several cycles of adsorption and desorption.[19] Calcium oxide based adsorbents result in metal carbonate in absence of water, whereas lithium oxide based adsorbents form hydrocarbonate phase in the presence of water. The former ones are advantageous in consideration of low cost and abundancy of its precursors on earth.[19] The latter ones have very selective CO_2 adsorbing mechanism and thermally stable at extreme temperature.[23]

Physical adsorbents comprise carbonaceous materials, zeolites, ordered mesoporous silicas, activated carbons, and MOFs. By the van der Waals force from internal pressure and molecular interaction, they physically adsorb CO_2 mainly in their high porous structure based on their shape selectivity, size selectivity, and adsorption selectivity. [24] Zeolites, microporous crystalline minerals comprising of hydrated aluminosilicates, have been extensively applied to the various separation process due to its high capability in molecular sieving.[25] Compared to other adsorbents including hydrotalcite, zeolite-based materials have shown high adsorption capacities under relatively low operation temperature.[26] Among commercial zeolites, the molecular sieve 13x with highest pore size and volume is reported as the highest CO_2 adsorbent.[27] In addition, molecular sieve 13x regenerated under pressure swing adsorption (PSA) and temperature swing adsorption (TSA) can be utilized as a competitive adsorbent of CO_2, especially in low pressure (<25 psi).[28] This specific material is tested for the verification of laboratory-made breakthrough experiment, which is reviewed in Chapter III. Activated carbon, a carbon with activated adsorbing surfaces of mesoporous or microporous structures produced from the carbonization and activation of coals or industrial byproducts, has been widely accepted as a decent CO_2 adsorbent.[19] This is beneficial as it is less energy intensive in the process of regeneration than zeolite adsorbent.[29] MOF, a crystalline solid organic-inorganic hybrid framework connected with metal-ligand bonds, has recently emerged as a competitive CO_2 adsorbent.[30] This has numerous advantages in the control of pore size, pore shape, and adsorbing surface to give rise to high selectivity, kinetics, and capacity, respectively.[31]

However, plentiful issues remain to be solved. The issues regarding (1) pressure drop, (2) equipment corrosion[20], (3) solution degradation[32], (4) large equipment size[9], and (5) large regeneration energy[33] have been troublesome when it comes to using amine solution such as MEA and DEA, the conventional representatives of the CO_2 absorbent. Not only is considerable heat needed to regenerate the absorbents, but also the inhibitors[34] are necessary for corrosion control. MEA itself is not so much corrosive, but degenerated intermediates intensify the corrosion.[35] Some adsorbents including lithium zirconate have drawbacks in adsorption/desorption kinetics.

As strong alternative, physical adsorbents including hollow fiber absorbents and ZIFs have notably achieved low pressure-drop, high stability, and low regeneration energy due to their inherent porous matrix, the property of solid, physical uptake and release, respectively.[36] However, a major concern of physical adsorbents, however, is both low stability and low capacity in the presence of water although water production in fossil fuel combustion is unavoidable. H_2O is, in fact, one of the major components that can competitively adsorb on the active sites of zeolite[19], activated carbon[37], etc. Especially, activated carbon suffers gradual oxidation of the carbon surface.[38]

In addition, the massive production for commercial plant is also of paramount importance.[44] Therefore, new physical adsorbents with (1) low regeneration energy (2) sustainable performance in the presence of water, and (3) commercial viability are worthy of investigation, development and inclusion in existing technologies.

1.3 Amyloid Biomaterials as Materials of the Future

Mother Nature has developed diversified methods to sequestrate CO_2 for its own sake.[39] To obtain energy source from CO_2, water and light, microorganisms have evolved original CO_2 concentration mechanisms, CO_2 fixation pathways, and CO_2 utilization methods.[40] Improvement in genetic engineering enables microorganisms to produce objective bio-based products. Biological absorbents have been traditionally based on photosynthetic organisms, which assimilate CO_2 to the complex molecules and consume such as energy sources. [41]

Recently, synthetic biology-based approach has been noticed due to the potential to develop a functionalized complex entity.[42] Biological molecules functionalized to capture CO_2 are regarded as one of the stronger alternatives. The focal point of such method is that specific design can be purposefully implemented on a molecular scale. [42] This readily satisfies several principles of Green Chemistry proposed by Tang et al. in that the fabrication process gives rise to (1) degradable chemical product, (2) few auxiliary substances, and (3) the low toxicity of chemical products. [43] Additionally, most of biological molecules come from (4) safe synthetic methods. Moreover, in the long term, bacterial production of DNA cloning potentially paves the way for the massive commercialization of peptide.[44]

Thermal and chemical stability mostly cause a hesitation to use protein as the adsorbent for anthropogenic sources with high temperature and harsh components. The amyloid biomaterials have been suggested as strong alternatives that overcome such drawbacks of current adsorbents.[44, 104] In this paper, amyloid biomaterials are based on the peptide scaffold inspired by the adenovirus fiber shaft. The introduction, challenge, and achievement of functionalized amyloid biomaterial from computationally designed peptide for capturing CO_2 are minutely discussed in Chapter II.

2. LITERATURE REVIEW

2.1 Nature of Self-Assembly

Self-assembly refers to the spontaneous arranging procedure that leads several basic elements into a highly organized scheme.[45] This intriguing phenomenon occurs without intervention from an outside source. The meaning of 'self-assembly' is not synonymous with 'formation'; the former can be controlled by how the components are organized, whereas the latter is not.[45] Amidst size variety in self-assembly, molecular self-assembly has attracted significant attention because engineering techniques in a top-down manner have faced a limitation over downsizing. However, self-assembly enables fabrication of highly ordered materials or formation from simple subunits with nanoscale or microscale size.[46] Molecular self-assembly stems from the implicit characteristics imposed by the non-covalent interactions.[45] These lead molecules to have supramolecular interaction, triggering a group of interesting properties in a material.[47] The engineering techniques based on the self-assembly have been extensively applied to the crystallization in all scales and the nanofabrication of robots, wires, protein films, chemicals, microelectronics, surface coating, and netted systems. [48]

2.2 Self-Assembly in Biological Systems

Self-assembly has triggered the complexity and functionality of biological systems from the basal building blocks. For instance, it has been found that DNAs can serve as excellent elementary units for the application of nanotechnology.[49] With a programmable ability for molecular recognition and microscopic size consisted of 2 nm of diameter and 3.4-3.6nm of the helical pitch, DNAs self-assemble in a remarkably controllable way.

Another example would be protein self-assembly. Several classes of proteins such as α-synuclein[50], a heterotetrameric diiron protein[51], and viral capsid protein[52] are known as building blocks that can self-assemble into crystal, filaments, gel, and other proteineceous aggregates with different scales and symmetries.[53] The self-assembling proteins not only play an important role in various physiological systems, but also allow the industrial application in the form of functional biomaterials.

Particularly noteworthy, peptides can perform as attractive building blocks for a wide range of new biomaterials. With the cooperation of non-covalent interactions, the self-assembly of peptides can be controlled in a kinetic and structural manner.[54] Hydrogen bonding plays a role of stabilizing the peptide's secondary structure and protein folding. Hydrophobic interactions can lead to a formation of micelles[55] and enhance the salt-triggered self-assembly due to the charge-screening effect.[56] Interactions between charges can be used for layer-by-layer self-assembly.[57] van der Waals interactions are not predominant but contributes to various non-covalent interactions.[54] Kinetic factors involving temperature and pH are strong factors that determine non-covalent interactions.[54] The suitable combination of such non-covalent interactions enables a controllable self-assembly of peptides. The rational selection of self-assembling strategies enables the fabrication of peptide biomaterials over different length scale with various functions.

2.3 Self-Assembling Peptide Biomaterials

Peptide as a scaffold of biomaterial has numerous advantages in terms of programmable structure, biocompatible and biodegradable property[58], versatile functionality[48] and top-down availability[59]. In the primary stage, Zhang suggested self-assembly of short designed peptides in aqueous solution by alternating the location of positive and negative charged amino acids to subsequently self-assemble those into

nanofibers making β-sheet structures.[60] Self-assembly of a series of nanoscale tubules described by Bong and Ghadiri is another quintessential example for purposely-designed peptides.[61] By alternating D- and L-amino acids, they possess a flat ring-shaped conformation to peptides, which are stabilized in an anti-parallel β-sheet formation through hydrogen bond interactions between the peptide backbones. Nowadays, the application of peptide comprises biologically compatible scaffold[62], non-lipid biological surfactant[63], and drug delivery system[64]. Moreover, novel robust biomaterials with functional nanostructures have been fabricated using amyloidogenic β-sheet self-assembling peptides.[65] The property of amyloidogenic β-sheet self-assembly is discussed in the following section minutely.

2.4 Amyloidogenic β-Sheet Self-Assembly

Amyloid nanostructures represent proteinaceous aggregates that can be deposited in tissues or organisms, which can lead to several pathological diseases including Alzheimer disease or type-2 diabetes.[66] Amyloid protein is hypothesized to build up in organs or tissues and decrease the physiological function of a normal protein by being unnecessarily accumulated around specific sites.[67] There has been great momentum to investigate the property of amyloid nanostructures for understanding the mechanism of amyloid formation.

The amyloid peptides with the specific sequence form β-Sheet through amyloid nucleation dependent polymerization and result in long fibers.[68,69,70] On the process of self-assembly, structure changes over from the normal fold of aggregated proteins to the β-sheet secondary structure. Fibril fragmentation is a dominant secondary process that forms fibril, consisting of lag phase and growth phase.[71] The time for the whole process to form fibril can shorten by the addition of fibrils seed, which cuts down the duration of the lag time.[72]

Amyloid fibrils have a cross β spine, which is a double β-sheet, with each sheet formed from side-by-side segments stacked.[73] Amyloid spine from various sequences is a pair of β-sheets with various classes of a dry steric zipper; interdigitation of side chains between parallel or antiparallel β-sheets causes the eight distinct classes of steric-zipper interaction.[74] These studies brighten the promising applicability of amyloid fibril based on its stability, self-assembling characteristics, and polymorphic structures. Amyloid proteins show a wide range of common properties owing to such plentifully interesting structures including elongated formation[75], β-sheet formation dyed by Congo red staining[76] and Thioflavin T[77], and unusual mechanical and chemical stability under the harsh environmental condition[78] due to the stacking of aromatic side chains. [79]

2.5 Properties of Amyloid Fibrils

The mechanical strength of amyloid fibril (0.6 ± 0.4 GPa) is paramount to that of steel (0.6-1.8 GPa) and silk (1-1.5 GPa). [80] This scaffold is also revealed to endure up to 100℃ of temperature. [81] Figure 2-2 shows the dimension of amyloid fibril by cross-β X-ray Diffraction pattern. [82]82 The whole fibril is around 100 Å in diameter, which is in the range from 40 Å to 120 Å. It typically shows lengthy, straight, and unbranched formation. In the parallel sheet, one strand is 4.8Å away from another strand right next to the one.[83] In the antiparallel sheet, strands are separated 9.6 Å. In terms of distance between sheets, one sheet is 10 Å away from another sheet beside the one. The amyloid structures have components in common consisted of 1) cross-β type β -strands horizontally lying to the fibril axis, 2) β -sheets as parallel or anti-parallel, and 3) the sheets in which strands line up with each other.[82, 84] Each different amyloid fibril morphology relates to different basic molecular structures where the main structure can be manipulated by variations in the condition of fibril formation. [85]

2.6 Current Amyloid Biomaterials

Based on the pragmatic properties in the section above, amyloid nanostructure can be applied to the development of functional amyloid biomaterials. Nature has explored functional amyloid fibrils for various applications. For instance, *E. coli.* curli operons forms amyloid fibrils to bind to host surfaces.[86] Yeast prions utilize amyloid fibril formation to evade cell death.[87] Pituitary secretory granules store hormone in a form of amyloid protein.[88] Furthermore, amyloid fibril biomaterials have been explored by researchers for specific purpose. The development of amyloid biomaterials is on the way to exploit its versatileness. Fibril has been regarded as a biocompatible matrix for tissue engineering, which can be applied into cell adhesion[89] or 3D cell culture systems[90]. Performance as a means of drug delivery is also promising in respect of the slow release [91] and the extended activity in vivo [92]. Metal nanoelectric material [93] and nanowire [94] are also self-assembled with advantages in clear synthesis and biodegradability.

2.7 Novel Amyloid Biomaterials Inspired by the Adenovirus Fiber Shaft

The sequence segments from the adenovirus fiber shaft have been deemed as motifs for novel biomaterial. The adenovirus type2 (Ad2) fiber trimers comprise three main segments: an N-terminal tail, a thin fibrous shaft, and a C-terminal globular knob.[95] The essential peptide residues that directly relates to the formation of self-assembling amyloid-like fibrils have been clarified in a minimalistic view. A stable domain of Ad2 fiber spanning residues 319-582 was identified and crystallized, unveiling a triple β-spiral fibrous fold for the shaft.[96] Furthermore, Papanikopoulou et al. found that five peptides from the adenovirus fiber shaft with lengths of 41, 25, 12, 8, and 6 self-assemble into amyloid-like fibrils. [97] They experimentally verified the formation of

amyloid-like fibrils using Congo red binding, electron microscopy, infrared spectroscopy and X-ray fiber diffraction methods. The sequences of five peptides are as follows.

41-amino acid peptide: PIKTKIGSGIDYNENGAMITKLGSGLSFDNSGAITIGNKND

25-amino acid peptide: AMITKLGSGLSFDNSGAITIGNKND

12-amino acid peptide: LSFDNSGAITIG

8-amino acid peptide: NSGAITIG

6-amino acid peptide: GAITIG

Remarkably, the amyloid-like self-assembly of peptide sequences, octapeptide NSGAITIG and hexapeptide GAITIG, are studied by Tamamis et al.[98] The results, including molecular conformation and fiber diameter, are in line with the experimentally observed data. They showed that modification of such peptide building blocks, particularly on N-terminal residues Asn1 and Ser2 that are exposed at the exterior of fibril and accessible, retains the amyloidogenic properties of peptide and imposes a binding function for metallic nanoparticles. This opens an applicability of utilizing MD simulations for the rational modification of new adenovirus fiber shaft. Based on this work, Kasotakis et al. showed that amyloid biomaterials formed by peptide NSGAITIG binds to gold nanoparticles, whereas amyloid biomaterials formed by peptide NCGAITIG, CNGAITIG, and CSGAITIG binds to gold, silver, and platinum nanoparticles.[99] They experimentally investigated that the N-terminal residues of octapeptide NSGAITIG can be substituted to the functional amino acids without harming the fibril-forming potential of peptides, and that the amyloid biomaterials formed by such peptides embody selective binding function to metals.[99]

Furthermore, Tamamis et al. studied the MD simulation of the dodecapeptide LSFNDSGAITIG from the adenovirus fiber shaft.[100] Tamamis et al. also investigated an aqueous solution of aspartate-rich peptide sequence LSGSDSDTLTV from the adenovirus fiber shaft. [101] As this sequence contains plentiful aspartate and serine, this is

designated to help the computational analysis of interactions to facilitate the nucleation of calcium ions and biomineralization.

Kasotakis and Mitraki also reported that the effect of serine residue onto NSGAITIG biomaterial incubated with TEOS precursors nucleate silica nanoparticles on the surface of such fibril.[102] They suggested the mechanism in which the serine residue is atypically rendered nucleophilic via hydrogen atom transfer by the N-terminal amino group.[102] Correspondingly, Terzaki et al. found the strategy for hard tissue engineering named ‘scaffold on scaffold’, referring that mineralized peptide tied to laser-made material enhances the proliferation.[103] Deidda and Jonnalagadda rationally designed and validated functional peptide RGDSGAITIGC that can potentially have functions of cell adhesion and cysteine-mediated functionalization properties.[104]All these results above illuminate the usefulness of rationally designed self-assembling peptides as a template for specifically oriented targets.

2.8 Computational Investigation of Structure of Amyloid Biomaterials

For a guide of the theoretical investigation of fibril-forming peptides, the case study of dodecapeptide LSFNDSGAITIG and octapeptide NSGAITIG (residue 385-392) by Tamamis et al. are briefly introduced in this chapter.[105] The following steps are the computational investigation including setup, execution and analysis of MD simulations of fibril-forming peptides, which elucidates the structure of amyloid biomaterial.

1. The representations for molecules and force fields are selected for the interaction between peptide and solvent.
2. All simulations are conducted with the CHARMM program[106] in this case study.
3. All simulations are conducted at infinite dilution condition for the prediction of implicit-solvent model.
4. The implicit solvent simulation results should be compared with the explicit solvent simulation results using REMD method[107] in the case without experimental information.
5. Container volume is adjusted to the experimental self-assembly concentrations and the non-bonded cutoff distance between peptides after the random placement of peptide over container.
6. Simulation with REMD method[108] is conducted under the satisfaction of several criteria (Temperature[109] and MD Steps[110]) and the fine-tuning of simulation condition (various temperature, replica with random walk, etc.).
7. The probable formation of intermolecular structures (β-sheets) is observed.
8. The intermolecular structures trajectories are visualized with the secondary-structure algorithms such as STRIDE[111] and DSSP[112].
9. Compare of the trajectories from infinite- and finite-dilution by merging coordinates.

Computational investigation for the detailed identification of intermolecular β-sheets are provided in the below. These are to figure out the richness of β-sheets content in a systematic way to analyze how much designed peptides are amyloidogenic.

1. The intermolecular β-sheet contents of aggregate are collected by post-processing trajectories.
2. β-sheet structures are classified in order of decreasing complexity using FORTRAN programs.
3. Detailed information is obtained by 2D probability maps of intermolecular β-bridges. "In" or "Off" register β-sheets are analyzed to find whether those are in states of antiparallel, mixed, and parallel.
4. Extra information on key sheet-stabilizing side chain interactions is obtained by probability maps of intermolecular side chain contacts.
5. New variables are introduced to identify different peptide shapes: Linear (I) or Bent (U).
6. The polar (P1) and nematic (P2) order parameter[113, 114] are introduced to reflect the orientation. The P1 and P2 are computed with the program WORDOM[115].
7. Free-Energy Landscape (FEL) are constructed by 2D probability as
$$G(P1,P2) = -k_bT * \ln P(P1,P2).$$
8. Representative structures are extracted from the FEL minima.
9. The global minimum strand folding is checked whether it is in agreement with the experimental width.

From this protocol, Deidda and Jonnalagadda et al. [104] developed self-assembling peptides as promising agents for tissue engineering. This clearly shows that the computational protocols are powerful tool for the development and fabrication of novel biomaterials. All peptides for novel amyloid biomaterial capturing CO_2 are computationally designed following an in-house protocol of Tamamis lab at Texas A&M

University. GAITIG and GAIIG scaffold are used as a source of inspiration for the novel amyloid biomaterials. The protocol is not provided here, as it is unpublished. The fabrication procedure of the amyloid biomaterials is discussed in 4.1.

2.9 CO_2 Capture Using Amyloid Biomaterials from Previous Studies

It was reported that hydrophobic dipeptides self-assemble crystal and nanochannel structures with low density.[116] To capture CO_2 with such material, porous dipeptide crystals with high selectivity on CO_2 over N_2 and CH_4 were produced and verified by isotherms, GCMC, and MAS NMR spectroscopy.[117] The dipeptides formed nanochannels through charge-assisted hydrogen bonds between ammonium and carboxylate groups, which leads to the physically selective capture of CO2.

Noticeably, amyloid biomaterials were fabricated for the purpose of CO_2 capture. Inspired by the aspect that Hemoglobin uptake CO_2 using its amine groups and that the regeneration energy of amines can be lowered if solid-supported, amyloid biomaterials formed by peptide VQIVYK are designed for selective CO_2 capture. [118] They utilized the epsilon-amino group of the lysine residue to form carbamate with CO_2.[119] Unlike the conventional stoichiometry (2:1) of CO_2 capture by a primary and a secondary amine[120], it shows 1:1 stoichiometry where one peptide binds to one CO_2 molecule. Chemical equations suggested for those reactions are described below. Figure 2-1 shows Zwitterion mechanism that is typically happened to primary or secondary amine. Figure 2-2 shows how an unexpected ratio was observed.

$$RNH_2 + CO_2 \rightleftharpoons RNH_2^+COO^- \quad [1]$$

$$RNH_2^+COO^- + RNH_2 \rightleftharpoons RNHCOO^- + RNH_3^+ \quad [2]$$

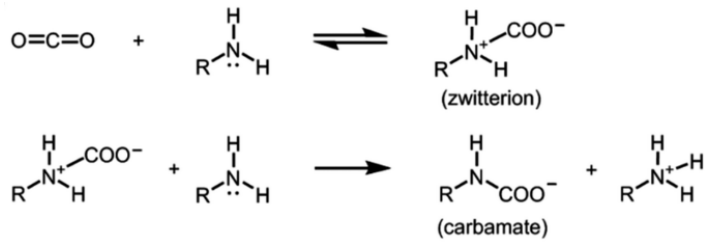

Figure 2-1. Zwitterion Mechanism proposed by Caplow[120]

$$RNH_2 + CO_2 \rightleftharpoons RNH_2^+COO^- \quad [3]$$

$$RNH_2^+COO^- + B \rightleftharpoons RNHCOO^- + BH^+ \quad [4]$$

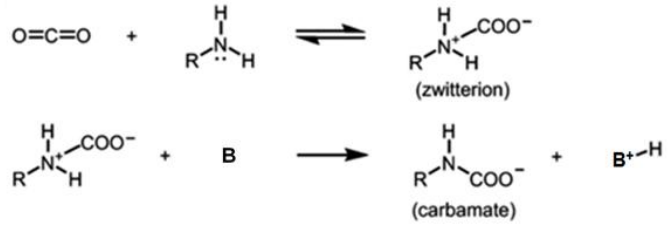

Figure 2-2. Carbamate Formation Mechanism proposed by Li et al.[118]

In Equation 1, the sorbent with the primary amine group, RNH_2, formulates the carbamic acid, $RNH_2^+COO^-$. However, as the reactants are not stable enough, these can react with another amine group, and sequentially build up carbamate, $RNHCOO^-$, and RNH_3^+ as in Equation 2. This is a typical reaction in amine-based sorbents; however, Li et al. proposed the mechanism as Figure 2-1 based on their experimental observation. To neutralize the amine group in lysine residue by making the carbamic acid stable, a high basic condition of sodium phosphate buffer (pH = 12.0) is used. As the basicity of added basic sodium phosphate buffer is higher than the basicity of amine group in lysine, the reaction of Equation 4 is preferred to the reaction of Equation 3.

This work manifested the potential of amyloid fiber as an adsorbent for CO_2 capture. Li et al. additionally suggested the structure-based designing approach of functional amyloid biomaterials formed by peptide LKQALKL, KLVFFAK, and VKAVAK, which show better binding capacities than their previous result of amyloid biomaterial formed by VQIVYK.[121] Steric zipper spines with inward-facing side chains[74] are selected and modified in order to increase hydrophobicity, neutralize pH, and modifythe size. High hydrophobicity helps form a stable fibril in the water. Neutral pH condition is important to make fibrils formed inmild pH.[121] For instance, Serine is substituted by Valine, and Asparagine is changed to Isoleucine for high hydrophobicity. For pH neutralization, Glutamic acid is substituted by Glutamine, and Aspartic Acid is replaced to Asparagine. To modify the size, floppy ends such as Thronine and Glycine are cropped. To increase CO_2 capture capacity, Lysine is inserted instead of the segments that do not consist of zipper spine. After this process, fibers are functionalized by supplanting side chains connected to the zipper spine and extending termini, both with functional amino acids. The group also found optimized pH condition by observing morphologies, checking fiber formation and estimating capacity of designed peptides synthesized from different pH. They obtained amyloid biomaterial formed by peptide KLVFFAK with doubled capacity compared to the one formed by peptide VQIVYK, which corresponds to the fact that the former contains two lysines. However, they also observed that the amyloid biomaterial formed by VQIVYKK has less than doubled capacity of amyloid biomaterial formed by peptide VQIVYK due to the adjacency of two lysines. This work explicates versatile applicability of amyloid biomaterial designed from a structure-based approach.

3. EXPERIMENTAL SETUP

3.1 Amyloid Biomaterials Preparation

All peptides are custom synthesized by Wuxi Apptech China and were utilized as a TFA salt as soon as received. The peptide powders were dissolved in 50mM sodium phosphate buffer of pH 8 with 6mg/mL concentration. All the peptide solutions were incubated in an ambient condition for three days. Fiber formation was verified by FESEM and TEM at Crete University in Greece. Fibrils were collected after the centrifugation at 13000 rpm for 30 min and resuspended in pH 12.6 of 50mM sodium phosphate buffer 50mM. The fiber solution was incubated at room temperature under agitation for 6 hours. Then the solution is lyophilized until the sample became a dry white powdery fiber. This step is to stabilize peptides by evading possible degeneration pathways.[122] The lyophilized fibril and salt powder was stored in the glass vacuum desiccator at room temperature. The lyophilized white powders are shown in Figure 3-1.

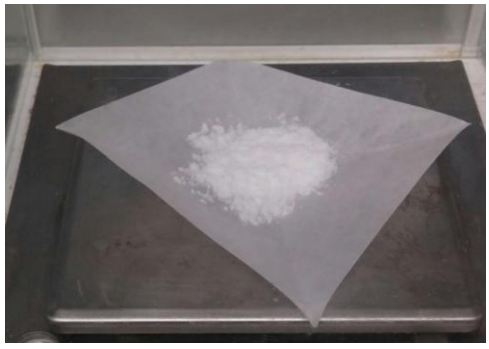

Figure 3-1. Amyloid Biomaterial in Lyophilized Powder Form

Amyloid biomaterials from five different peptides are fabricated. Specific sequences of such biomaterials will be claimed in the journal that will be peer-reviewed and published hereafter. To help classification, each amyloid biomaterial is named amyloid biomaterial formed by peptide 1, amyloid biomaterial formed by peptide 2, etc.

3.2 Breakthrough Measurement System

Breakthrough measurements in the presence and absence of water are laboratory-made and performed to evaluate the dynamic CO_2 separation capacity of the biomaterial. The schematic diagram of breakthrough measurement and its actual setup in the laboratory are described as follows in Figure 3-2. The setup inside the adsorption bed is also depicted. Figure 3-3 shows the photo of actual setup of breakthrough measurement system.

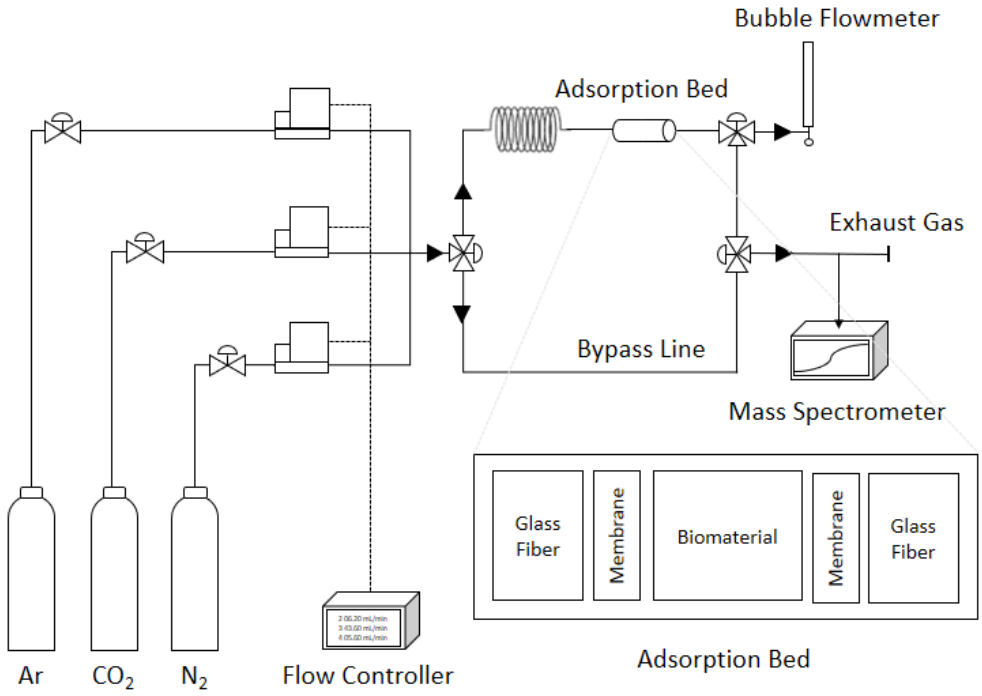

Figure 3-2. Schematic Diagram for Breakthrough Measurement in Absence of Water

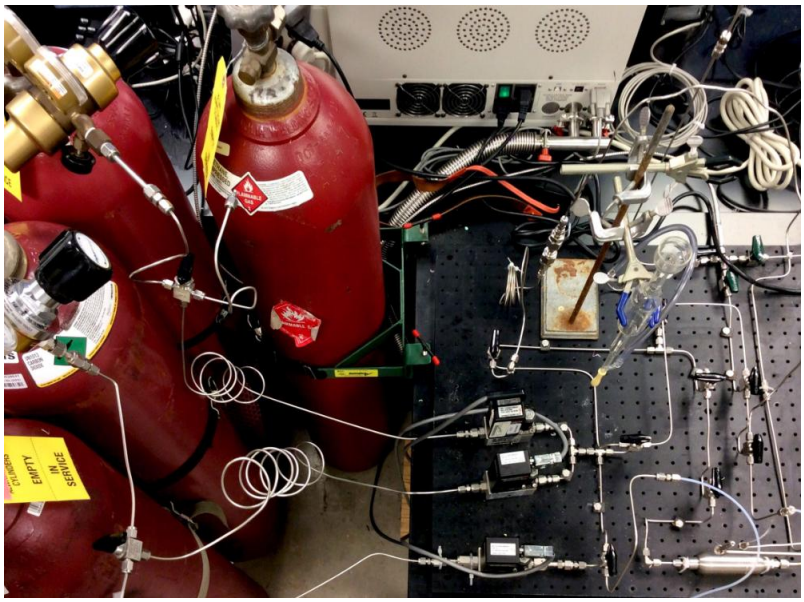

Figure 3-3. Setup of Breakthrough Measurement System

The brief illustrations in chronological order are described as below in Figure 3-4.

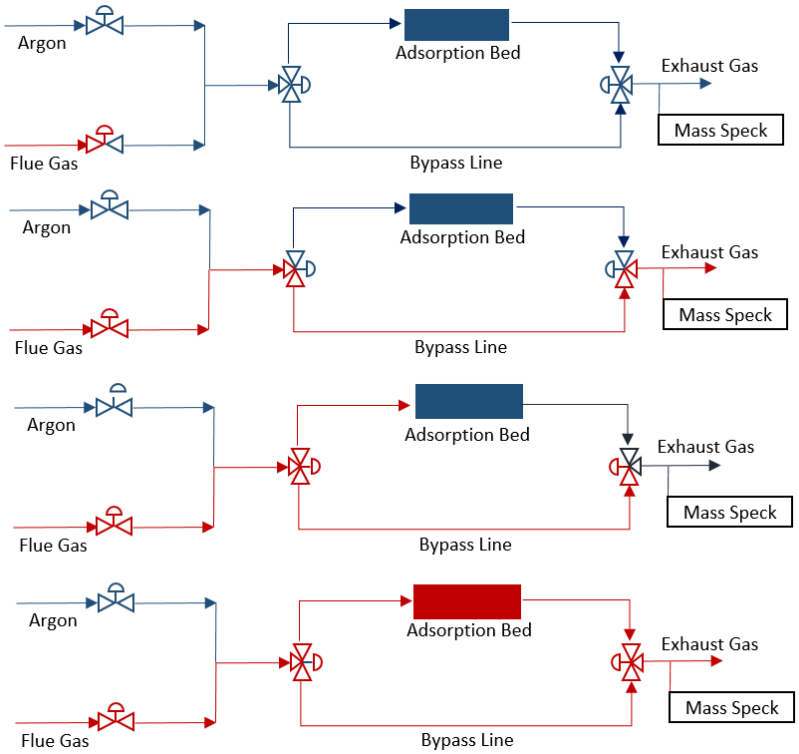

Figure 3-4. Illustration of Breakthrough Measurement in Absence of Water

The adsorbent is exposed to a flue gas stream to evaluate how long such materials take for selective capture of CO_2 while nitrogen intactly passes it through. The adsorbent material is homogeneously packed in stainless steel tube (1/2”OD, 0.049” Wall Thickness × 2 inch, Swagelok). The vacant portion in the bed is filled with trimmed fiber glass wool (Corning, 8μm), an inert material that does not selectively react, adsorb, and absorb inlet gasses. Wool acts as a physical filter that prevents adsorbents from being swept away by the momentum of inlet gas flow. However, contact of biomaterial with glass wool can also lead to some weight loss. Therefore, microporous membranes (Millipore, Filter type: 0.05μm) with selectivity on neither CO_2 nor N_2 are inserted between glass wool and material to maximize the recovered amount of biomaterial.

As with the total procedure, Argon flow is first used to flush the whole system and the adsorbents. Flue gas then flows through bypass line in order to check the constant composition of flue gas. After reaching out to dynamic equilibrium of such composition, the flow directions toward bypass line are changed to the adsorption bed to start seeing breakthrough over adsorption bed. Pressure drop and temperature change here are assumed negligible, as the packing amount throughout the experiments barely affects the surrounding pressure and temperature.

Flue gas consists of nearly 14% CO_2 (v/v) and 86% N_2 (v/v), which simulates the composition of flue gas from a general power plant. A mass Spectrometer (Hiden Analytics, QGA-gas analysis system, Software: MASsoft 7) is used for the analysis of the gas composition which passed the packed bed. The calibration method is discussed in the 3.4. The mass flow controller (BROOKS, 5850E) is directly connected to a flow controller (BROOKS, 0154E) to designate a specific flow rate. Argon flow rate is measured by using the highly accurate bubble flowmeter. A flue gas of specific flow rate with such ratio is confirmed by using soap film flowmeter (Hewlett Packard, 100ml, 0101-0113) and mass spectrometer repeatedly.

3.3 Preparation of Humid Condition

The schematic diagram of breakthrough measurement in the presence of water is described in Figure 3-5.

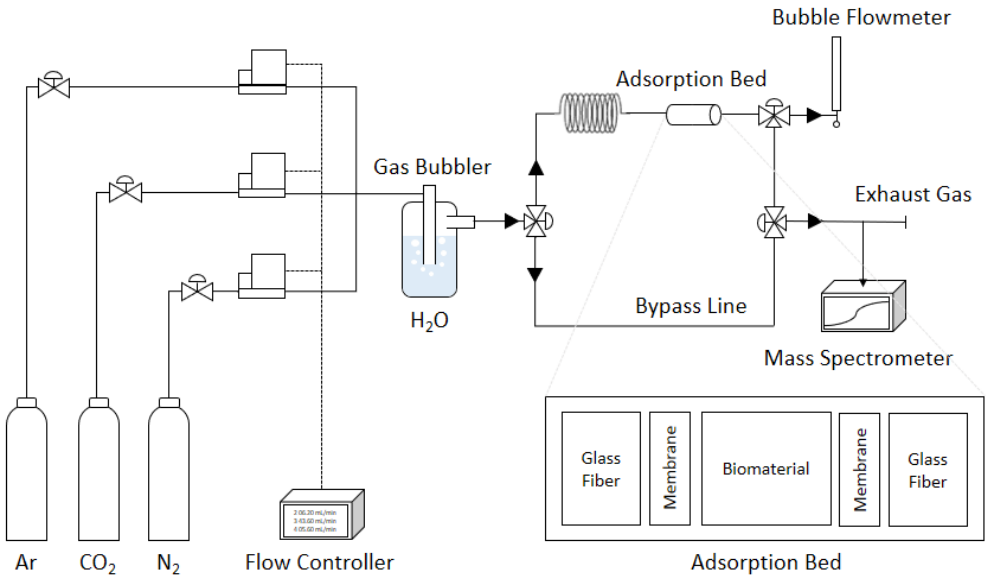

Figure 3-5. Schematic Diagram for Breakthrough Measurement in Presence of Water

Humidifying apparatus (Labglass, 500mL) is set up between the inlet gas and the valve before adsorption bed and bypass line. This generates 100% relative humidity, which is tantamount to 1.49% (w/w) of water moisture. Humid Nitrogen is equilibrated for 2 hours into the adsorption bed.[118] The humidifier is detached before the flue gas is started to flow through the bypass line, and the remaining procedure is same as the breakthrough measurement in the absence of water. This procedure is to investigate that the breakthrough cycle is reproducible regardless of humidity in the flue gas. This process will be tested with the newly ordered samples.

3.4 Notes for Breakthrough Measurement Setup

Two issues are handled to specify those parameters:

1. In the case of flow rate less than 5 sccm, the driving force of flow is not enough to move the bubble layer outwards or to generate the bubble layer.
2. The mixing of 8.5 V (mL) of N_2 and 1.5 V (mL) of CO_2 does not confirm 10.0 V of Flue gas with 85% of N_2 and 15% of CO_2, as the moving speed of each gas is different as well as the mixing is not perfect.

Therefore, a staged approach is used to solve those problems. In the first stage, the flow rate of N_2 is measured and set to be 8.5 V. Additionally, certain amount CO_2 is specified through mass flow controller to make up total 10 V of flue gas. The composition is sequentially checked through the mass spectrometer to find whether it satisfies an objective value. If the composition deviates from such value, the whole procedure with edited set value can be repeated until the optimum value is obtained. This process is briefly described in Figure 3-6.

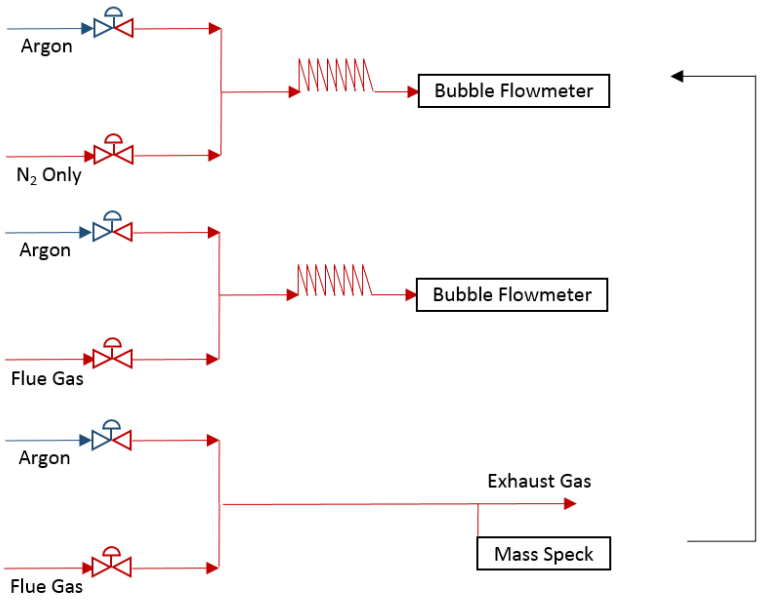

Figure 3-6. Procedure to Set Specific Flow Rate with Specific Composition

The QGA mass spectrometer was calibrated for the case of humid condition. The dry-bulb temperature and relative humidity is detected by VWR Jumbo Temperature/Humidity Meter. From the saturation pressure of the temperature indicated, the ambient pressure of water vapor can be calculated by the equation below.

$$\text{Ambient P of Water} = \text{Saturation P of Water at Certain T} \times \text{Relative Humidity (\%)}$$

Assuming the ideal gas law, it is clear that partial pressure of specific molecules is proportional to the number of specific molecules in unit volume. By comparing ambient pressure of water with standard pressure, water content is identified in terms of the number of molecules. Considering typical air composition without water contents, arranged composition at the condition of specific temperature and relative humidity can be derived. This value can be used for the calibration process of mass spectrometer.

Kelvin 0'C	**273**	**K**	**Dry Gas**	**98.58%**		
Temp	22	C	Typical Air Composition		Arranged Composition	
Dry Bulb T	295	K	N_2	78.03%	N_2	76.92%
Psat of H_2O	2612.018	Pa	O_2	20.99%	O_2	20.69%
Psat of H_2O	2.612018	kPa	CO_2	0.04%	CO_2	0.039%
Pstandard	101.325	kPa	Ar	0.94%	Ar	0.93%
Hrel	55	%			H_2O	1.42%
P of H_2O	1.43661	kPa				
Content	1.417824	%				

Table 3-1. Example of Arranged Composition Calculation at Certain Condition

3.5 Validation of Breakthrough Apparatus

The whole setup of breakthrough apparatus is validated through the experiments using commercial Molecular Sieve 13x (Micromeritics). This is to see whether the estimated capacity is compatible with the range of reported values. For free volume test, molecular sieve 13x was regenerated using BET activation process at 467K under high vacuum (~50μmHg) for 12 hours. Material regeneration method is described in the next section. Dead volume was measured using saturated and inactivated molecular sieve 13x. Breakthrough curves obtained by those conditions are plotted in Figure 3-7. Actual volume corresponded to 2.05 mmol/g of CO_2 uptake, which is compatible to the competitive adsorption results using CO_2 and N_2 at around standard pressure and temperature condition; by 2.1 mmol/g of Siriwardane et al[28], and 2.23 mmol/g of Lee et al[123]. The method to calculate CO_2 capture capacity is presented in the Chapter IV.

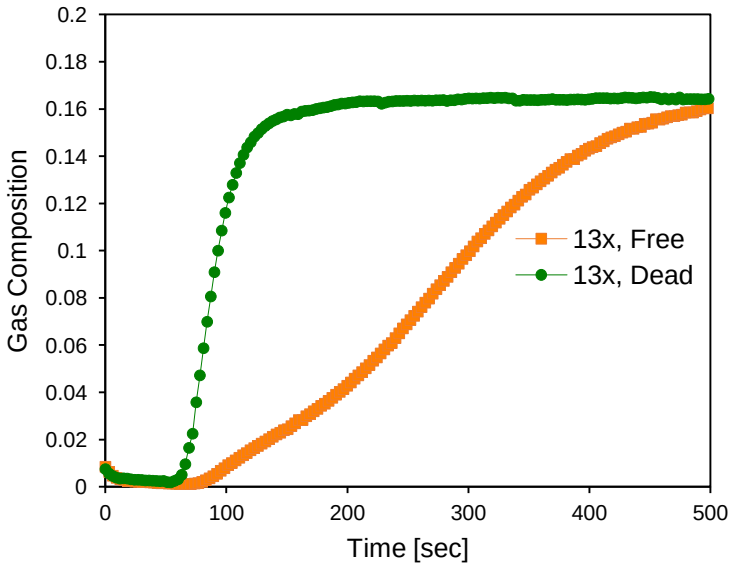

Figure 3-7. Breakthrough Curves for Free and Dead Volume of Molecular Sieve 13x

3.6 Material Regeneration Condition

Before the finalization of regeneration condition, attempts to use vacuum oven, in-situ bed heating, and BET activation process were made. It is turned out that the regeneration of amyloid biomaterials using the degassing process of BET Apparatus (Micromeritics, ASAP 2010, Figure 3-8) under the condition of mild heat (set point 100℃) and vacuum swing ($\leq 10\mu$mHg) is most promising. The temperature condition has followed the regeneration temperature of amine-based biomaterials.[118,121] Time condition is being confirmed from trial and error, which is discussed in Chapter IV. Temperature and pressure control and detection can be simultaneously executed through this apparatus. Vacuum swing adsorption is to detach the physically adsorbed CO_2 in the adsorbent, whilst temperature swing adsorption is to regenerate carbamate in the lysine to the amine functional group.[124]

Figure 3-8. BET Apparatus, Micrometrics ASAP 2010

4. RESULTS

4.1 Validation of β-Sheet Formation

Peptides' self-assembly properties were investigated using the in-house protocol of Tamamis lab introduced in 2.8.[105] REMD simulation snapshots in a water box were examined for the analysis. Residue participation in β-sheets per peptide are examined by the averaged amount of amyloidogenic β-sheet formation for each strand. Secondary structure β-sheet formation resulting from the replica exchange MD simulation snapshots of computationally designed peptide were evaluated using STRIDE[111] algorithm of VMD. The residue participation in β-sheets per peptide can be obtained by dividing the number of residues involved in β-sheets by the number of frames from simulation and the number of strands. Since the residues AITIG mainly take part in the β-sheet formation[98], averaged residue participation in β −sheets per peptide around four indicate that the self-assembled peptide is rich in β-sheets. The result as in Figure 4-1 suggested that all the designed peptides show the richness in β-sheets, verifying that the designed peptides are highly amyloidogenic.

$$Averaged\ Residue\ Participation\ in\ Beta\ Sheets\ per\ Peptide = \frac{The\ Number\ of\ Residues\ Involved\ in\ \beta - Sheets}{Number\ of\ Frames\ *\ Number\ of\ Strands}$$

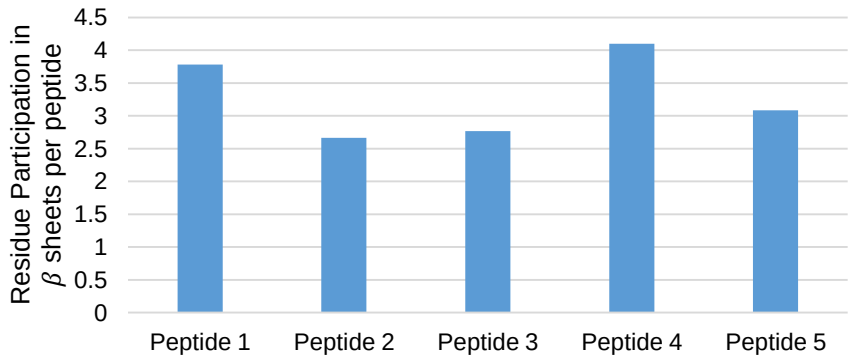

Figure 4-1. Averaged residue participation in β-sheets per peptide

4.2 Calculation Method for CO_2 Capture Capacity

To measure the CO_2 capture capacity, detection time delay on the breakthrough measurement is converted into the volume of CO_2 captured, referred to as free volume. However, this does not consider the time delay by the vacant space, referred to as dead volume, throughout the main line. Dead volume is typically calculated using the porosity and the volume of main line, which is assumed the volume of adsorption bed. However, for the case of the adsorbents that are impossible to measure porosity or have unknown porosity, dead volume can be evaluated using the fully saturated material. Mole adsorbed by the material can be calculated as follows.[125]

Actual Mole Adsorbed = the total moles adsorbed in free volume
– the total moles absorbed in dead volume (empty volume) (1)

$$n_{ads} = \frac{V_{CO2} P_{atm}}{RT} - \frac{V_{CO2,EV} P_{EV}}{RT}$$
$$= \frac{y_f Q_f t_t P_{atm}}{RT} - \frac{y_f \varepsilon_T V_b P_b}{RT_b}$$

However, when the adsorbents are atypical so that it is hard to determine its porosity, the equation below offers a nice apporach to calculate dead volume. If the adsorbent has high selectivity on CO_2 over N_2, then the total adsorbed amount becomes relevant only to the amount of adsorbed CO_2 if CO_2 and N_2 are only used. Therefore,

Actual Mole Adsorbed = the moles of CO_2 adsorbed by activated sample
– the moles of CO_2 adsorbed by saturated sample (2)

As saturated adsorbents barely captures CO_2, the latter term would mainly consider the effect of the dead volume, which means the volume of the pores in between particles and empty volume in the adsorbent bed. CO_2 on the saturated sample would not

be desorbed by sole inert gas flushing as Argon flushing needs to be done every single time before the breakthrough measurement starts off. The identically shaped material that does not capture CO_2 would be ideal to measure the moles of CO_2 adsorbed by saturated sample. In line with this point, the regenerated buffer can be also used to calculate the dead volume estimation.

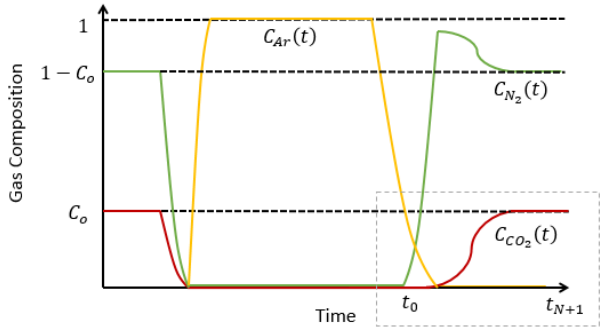

Figure 4-2. Typical Breakthrough Curves using Ar, N_2 and CO_2;
A Zone of Interest for Capacity Calculation is Grey-Boxed.

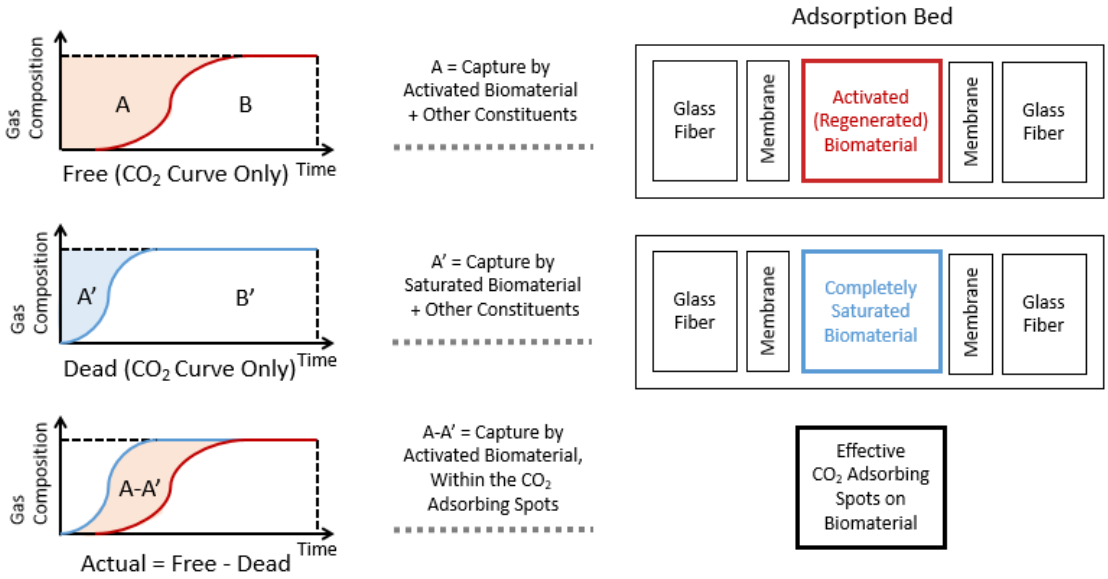

Figure 4-3. Free, Dead, and Actual Volume Adsorbed

Figure 4-2 shows the zone of interest for the calculation from the typical breakthrough curves. In Figure 4-3, Area A is a time [sec] that indicates the delayed time

by a capture of activated biomaterial and the vacant volume. Area A' is a time [sec] that shows the delayed time by a capture of saturated biomaterial and the vacant volume. By subtracting A' from A, the effective time that indicates a capture by adsorbing spots on biomaterial can be only taken into account. Figure 4-4 shows intuitively how to calculate an area of A from the raw data.

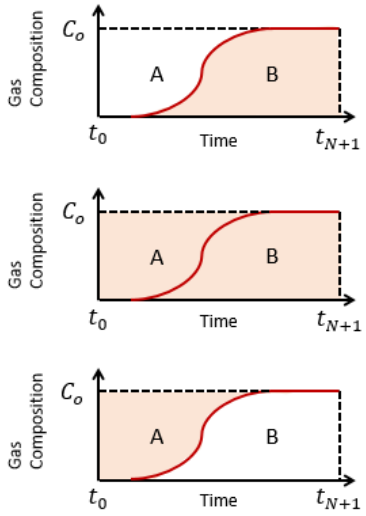

Figure 4-4. Obtaining an Area of A from CO_2 Breakthrough Curve

B can be calculated by the integration of CO_2 composition curve from the starting point of breakthrough to the ending point.

$$B = \int_{t_0}^{t_{N+1}} C_{CO_2} dt \ [sec]$$

As composition is given as a set of points in time step, this can be numerically intergrated applying Simpson's 3/8 rule as below. For most of the cases, the last point is selected where it corresponds to more than 500 seconds. This enables to have a reliable accuracy regardless of time step of mass spectrometer.

$$B = \int_{t_0}^{t_{N+1}} C_{CO_2} dt \ [sec] = \frac{3}{8} * \frac{t_{N+1} - t_0}{N+1} *$$

$$[C_{CO_2}(t_0) + \sum_{n=1}^{N/3} [3 * C_{CO_2}(t_{3n-2}) + 3 * C_{CO_2}(t_{3n-1}) + 2 * C_{CO_2}(t_{3n})] + C_{CO_2}(t_{N+1})]$$

The number of data selected to measure, n, is selected from the starting point of breakthrough to the point that shows the concentration equilibrium.

As A+B would be the area of rectangle, A can be calculated as below.

$$A + B = C_o * (t_{N+1})\ [sec]$$

$$\therefore A = (A + B) - B = C_o * (t_{N+1}) - \int_0^{t_{N+1}} C_{CO_2} dt\ [sec]$$

Actual delated time can be calculated from the colored areas of the activated and saturated sample as Figure 4-5.

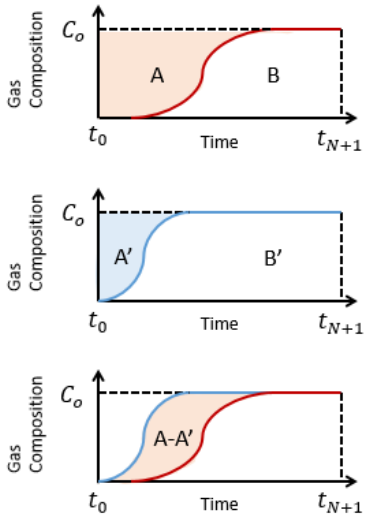

Figure 4-5. Obtaining an Area of Actual delay time from Free and Dead Curves

$$\tau_{Free} = A$$

$$\tau_{Dead} = A'$$

$$\tau_{Actual} = \tau_{Free} - \tau_{Dead} = A - A'$$

The actual time can be converted into the volume by multiplying total flow rate. Note that actual time is an integrated value of CO_2 composition over time, so it gives

CO_2 captured volume after multiplied to the total flow rate. This volume can be converted into the molar amount by applying the ideal gas law.

Dividing by the weight of biomaterial, CO_2 capture capacity can be evaluated in the unit of mmol/g or mL/g.

$$\tau_{Actual}\ [sec] * Q_{total}\left[\frac{mL}{sec}\right] = V_{actual}[mL]$$

$$\frac{V_{actual}[mL]}{1000} * \frac{\mathrm{P_{atm}}}{RT} * 1000 = n_{actual}\ [mmol]$$

$$C_{actual}[mmol/g] = \frac{n_{actual}[mmol]}{w_{biomaterial}\ [g]}$$

$$C_{actual}[mL/g] = \frac{V_{actual}[mL]}{w_{biomateiral}\ [g]}$$

As the capture mechanism is based on the functionalization of peptides, the CO_2 uptake per peptide should be evaluated as well. The 1:1 binding ratio of CO_2 and biomaterial is calculated by taking into account of the proportion of amyloid fibers in the whole material.[118]

$$Ratio_{peptide}[\%] = \frac{w_{peptide}\ [g]}{w_{biomaterial}\ [g]} = \frac{w_{biomaterial} - w_{corresponding\ buffer}}{w_{biomaterial}} * 100$$

$$MW_{biomaterial} = MW_{peptide} * (\frac{100[\%]}{Ratio_{peptide}[\%]})$$

$$C_{1:1}\left[\frac{mL}{g}\right] = \frac{V_{CO_2,\,1\,mol}}{MW_{biomaterial}}$$

$$N_{CO_2} = \frac{C_{actual}\left[\frac{mL}{g}\right]}{C_{1:1}\left[\frac{mL}{g}\right]}$$

4.3 Evaluation of CO_2 Capture Capacity

Buffer with high pH at as-synthesized state captures CO_2. As-synthesized amyloid biomaterial is not considered for the evaluation of CO_2 capture capacity. However, the buffer in amyloid biomaterial cannot be regenerated after the regeneration at 100℃ in vacuum, while peptide fibril in amyloid biomaterial can be regenerated after several cycles of regeneration. Therefore, the capacity after regeneration is a straightforward indicator to check the workability of functionalized peptide. This capture availability of biomaterial components at certain stages is tabulated in Table 4.1.

Biomaterial	As-synthesized	1st Regenerated	Nth Regenerated
Self-assembled Peptide Fibril	O	O	O
Phosphate Buffer with Certain pH	O	X	X

Table 4.1. Capture Availability of Biomaterial Components at Certain Stages

The capture of phosphate buffer at as-synthesized state is because lyophilized buffers at high pH have a high deliquescence due to Sodium Hydroxide. Sodium Carbonate is produced as soon as it is released to atmosphere through the acid-base reaction as follows. Since this is neither reversible nor easily decomposable in mild temperature, trials to regenerate samples at 100℃ are not effective at all.

$$2NaOH\,(s) \rightleftharpoons 2Na^+\,(aq) + 2OH^-\,(aq)$$

$$CO_2\,(g) + 2H_2O\,(l) \rightleftharpoons H_2CO_3\,(aq) + H_2O\,(l)$$

$$H_2CO_3\,(aq) + 2H_2O\,(l) \rightleftharpoons CO_3^-\,(aq) + 2H_3O^+\,(aq)$$

$$2Na^+\,(aq) + 2OH^-\,(aq) + CO_3^-\,(aq) + 2H_3O^+\,(aq) \longrightarrow Na_2CO_3(s) + 4H_2O\,(l)$$

Net Reaction: $2NaOH\,(s) + CO_2\,(g) \longrightarrow Na_2CO_3(s) + H_2O\,(l)$

Decomposition (~500℃): $Na_2CO_3\,(s) \xrightarrow{\Delta} Na_2O(s) + CO_2\,(g)$

Amyloid biomaterials formed by peptide 1 to peptide 5 showed most promising result in terms of CO_2 capture capacity after regeneration. Amyloid biomaterials formed by Peptide 2, 3 and 4, however, showed CO_2 capture in an as-synthesized state but showed limited CO_2 capture after regeneration. The results from amyloid biomaterial formed by peptide 1 to amyloid biomaterial formed by peptide 5 are mainly presented. Experimental data for amyloid biomaterial formed by peptide 1 are tabulated in Table 4-2. The number of CO_2 molecules captured per peptide of amyloid biomaterial formed by peptide 1 is described in Figure 4-6. Note that regeneration conditions are not consistent here since at the initial experiments several trials and errors were practiced to find an optimal regeneration condition. This will be discussed in the next section.

	Reg. Time in Vac Oven at 100℃	**Capacity [mmol/g]**	***N_{CO2} (# of CO_2 per Peptide)**
As-synthesized		-	-
1st Regeneration	2hrs	0.62	2.32
2nd Regeneration	2hrs	-	-
3rd Regeneration	1hr	0.20	0.77
4th Regeneration	1hr	0.20	0.78
5th Regeneration	0.5hr (BET)	0.19	0.73
6th Regeneration	0.5hr (BET)	0.11	0.43

Table 4-2. Tabulated Data for Amyloid Biomaterial Formed by Peptide 1

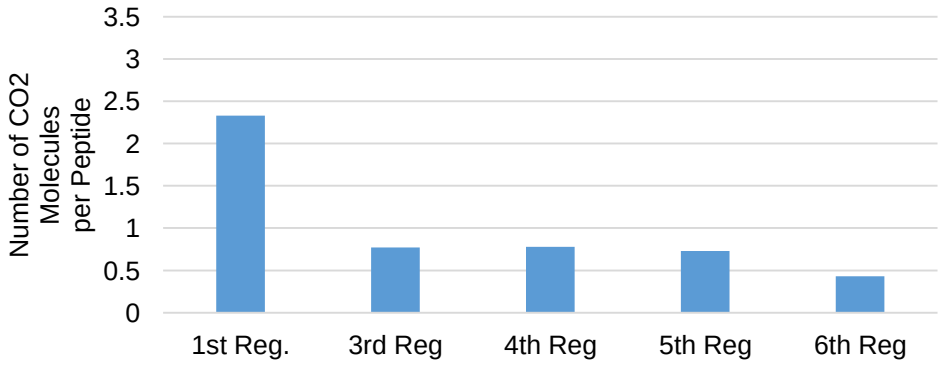

Figure 4-6. The Number of CO_2 Molecules Captured per Peptide of Amyloid Biomaterial Formed by Peptide 1

Amyloid biomaterial formed by peptide 1 at as-synthesized was not measured due to the malfunctioning of Mass spectrometer at that time. During the handling procedure, it was revealed to the air for a long time and showed no capture. Thus, amyloid biomaterial formed by peptide 1 was measured after the first regeneration. It shows capture more than 2 CO_2 molecules per peptide. Figure 4-7 shows the breakthrough measurement results, which clearly indicate the delay of CO_2 detection. Nevertheless, it shows steady degradation after regeneration cycles, and finally shows no capture after seventh regeneration.

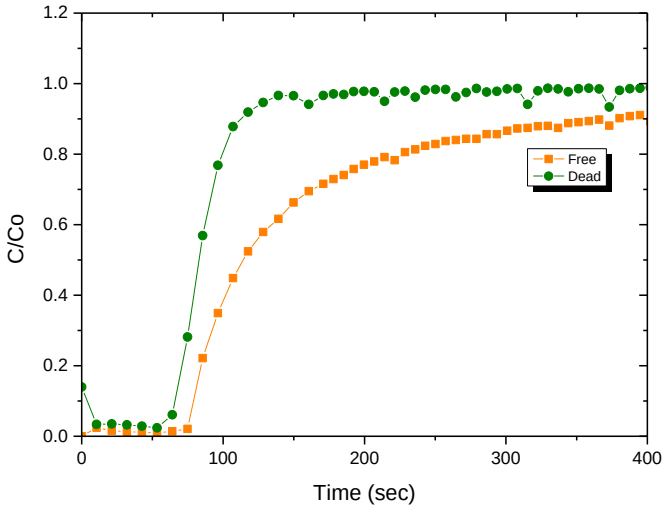

Figure 4-7. Breakthrough Curves of 1st Regenerated Amyloid Biomaterial Formed by Peptide 1

The experimental data of amyloid biomaterial formed by peptide 5 are tabulated in Table 4-3. The number of CO_2 molecules captured per peptide of amyloid biomaterial formed by peptide 1 is described in Figure 4-8.

	Reg. Time in BET at 100℃	Capacity [mmol/g]	*N_{CO2} (# of CO_2 per Peptide)
As-synthesized		0.74	3.19
1st Regeneration	17hrs	0.76	3.24
2nd Regeneration	23hrs	0.32	1.36
3rd Regeneration	0.5hrs	-0.11*	-0.50*
4th Regeneration	2hrs	0.05	0.23

**Overshoot occurred in the dead volume testing.*

Table 4-3. Tabulated Data for Amyloid Biomaterial Formed by Peptide 5

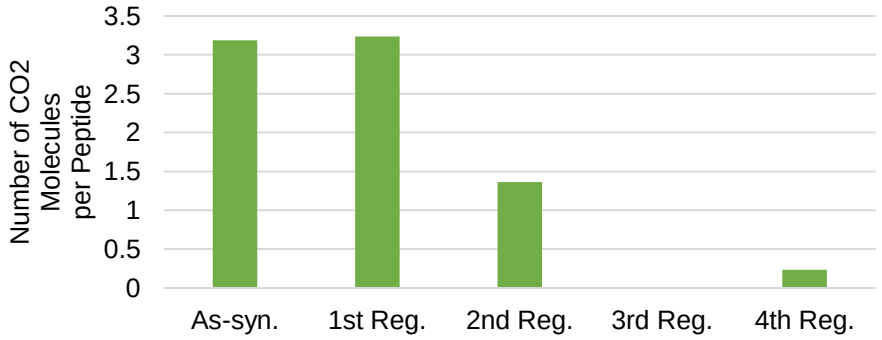

Figure 4-8. The Number of CO_2 Molecules Captured per Peptide of Amyloid Biomaterial Formed by Peptide 5

Amyloid biomaterial formed by peptide 5 shows nearly same amount of captures both in as-synthesized and 1st regenerated condition. Figure 4-9 is the breakthrough measurement results where actual delay of CO_2 detection clearly happened. As the dead volume of 1st regenerated amyloid biomaterial formed by peptide 5 is not measured after regeneration, as-synthesized dead volume is rather used for the calculation. This approximation is identified to be valid by checking other sets of amyloid biomaterials. The number of CO_2 molecules captured per peptide is evaluated as much as 3.24 CO_2 molecules. As it showed capture even after 17 hours of regeneration, 23 hours of regeneration was subsequently conducted in order to find the maximum capacity. However, the capture has been significantly reduced after the second regeneration, and the amyloid biomaterial formed by peptide 5 eventually showed significantly less

capture after third regeneration. This finding suggests that 23 hours of regeneration time possibly had a negative effect on the amyloid biomaterial formed by peptide 5.

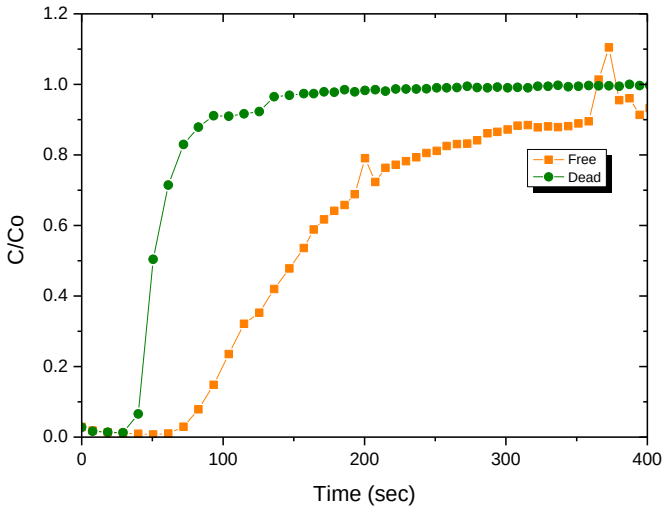

Figure 4-9. Breakthrough Curves of 1st Regenerated Amyloid Biomaterial Formed by Peptide 5 (Free) and As-synthesized Amyloid Biomaterial Formed by Peptide 5 (Dead).

4.4 Finding Optimum Regeneration Condition

For the continual use of adsorbent, material has to be fully regenerated under mild heating condition. Comparing the capacities after regeneration at certain temperature in vacuum oven or BET activation process, a proper regeneration condition is being determined. BET activation process with 100℃ of temperature at high vacuum (under 20μmHg) for 2 hours has produced reproducible results. However, the proper regeneration time should be confirmed, as it might not show a full capacity. Additional experiments have been conducted for the finalization of the optimum condition. The new condition considers the stability of biomaterial after repetitive regeneration cycles as well as the working capacity. The difference of characteristics between regenerated and saturated biomaterial could be subsequently investigated by the result of transmission electron microscopy (TEM), and powder X-ray diffraction.

5. CONCLUSION AND FUTURE WORK

Amyloid biomaterial based on computational design of peptide sequence are synthesized and evaluated to test CO_2 capture capacity. The material is considered as a strong alternative for CO_2 adsorbent, since amyloid biomaterials have moderate regeneration temperature, high stability during the regeneration cycles selectivity for CO_2 and water stability.[18,126] Promising five peptide sequences are obtained from the computational design that implements the mutation of residues in the way of both functionalization and stabilization. This peptide is ordered and is fabricated into the form of amyloid biomaterials by a self-assembly and the lyophilization of the mixture of peptide fibrils and phosphate buffer. Breakthrough measurement studies show that amyloid biomaterial from peptide 1 to 5 captures CO_2. Amyloid biomaterials formed by peptide 1 and 5 showed promising CO_2 captures after regeneration, but amyloid biomaterials formed by peptide 2, 3 and 4 showed limited capture after regeneration. The results of amyloid biomaterials formed by peptide 1 and 5 show that the CO_2 capture mechanism does not only rely on the capture of exposed arginine or lysine groups acting as amines. Although amyloid biomaterials from peptide 1 and peptide 5 showed good capture after first regeneration, those were gradually reduced after several cycles of regeneration. This suggests the necessity of the optimized regeneration conditions, especially in terms of regeneration time. Additional test using amyloid biomaterials are required for the finalization of regeneration condition and validating the computational design results. After the posterior computational validation based on the experimental results, the new peptides were ordered and will be tested soon. Breakthrough measurement in humid condition will be also conducted to verify the capture capacity in the presence of water.

Repeating research cycles from computational design to experimental validation can contribute to improve the computational design methodology of fibril forming functional peptides for the amyloid biomaterials. Check needs to be added to verify that

if designed scaffolds are antiparallel or parallel then the designed biomaterials show corresponding performance based on the antiparallel or parallel arrangement, respectively. CO_2 Adsorption Isotherm should be further investigated to understand the mechanism and dynamics of CO_2 adsorption and desorption through the type of its isotherm curve. Powder X-ray Diffraction, Transmission Electron Microscope, and Solid-State NMR will help to characterize the states from the saturated biomaterial to the regenerated biomaterial. This would also help confirm the occurrence of chemisorption by the carbamate. Correlation between the number of residue participation in β-sheet of designed peptides and the thermal stability of amyloid biomaterial formed by such peptides can be additionally investigated to develop more stable amyloid biomaterials. Comparison between the result of explicit simulation and implicit simulation will give an insight to have a better understanding of CO_2 capture.

REFERENCES

1. Davis SJ, Caldeira K, Matthews HD (2010), Future CO_2 emissions and climate change from existing energy infrastructure, Science, 329(5997):1330-3.

2. Barnett TP, Adam JC, Lettenmaier DP (2005), Potential impacts of a warming climate on water availability in snow-dominated regions, Nature, 438:303-309

3. Lashof DA, Ahuja DR (1990), Relative contributions of greenhouse gas emissions to global warming, Nature, 344:529-531.

4. Canadell JG, Le Quéré C, Raupach MR, Field CB, Buitenhuis ET, Ciais P, Conway TJ, Gillett NP, Houghton RA, Marland G (2007), Contributions to accelerating atmospheric CO_2 growth from economic activity, carbon intensity, and efficiency of natural sinks., Proc Natl Acad Sci U S A., 104(47):18866-70.

5. Hansen J, Sato M, Ruedy R, Lo K, Lea DW, Medina-Elizade M (2006), Global temperature change, Proc Natl Acad Sci U S A., 103(39): 14288–14293.

6. Raupach MR, Marland G, Ciais P, Le Quéré C, Canadell JG, Klepper G, Field CB (2007), Global and regional drivers of accelerating CO_2 emissions, Proc Natl Acad Sci U S A, 104(24):10288-93.

7. Panwar NL, Kaushik SC, Kothari S (2011), Role of renewable energy sources in environmental protection: A review, Renewable and Sustainable Energy Reviews, 15(3):1513-1524.

8. Herring H (2006), Energy efficiency—a critical view, Energy, 31(1):10-20

9. Haszeldine RS (2009), Carbon capture and storage: how green can black be?, Science, 325(5948):1647-52.

10. Yang H, Xu Z, Fan M, Gupta R, Slimane RB, Bland AE, Wright I (2008), Progress in carbon dioxide separation and capture: a review., J Environ Sci (China), 20(1):14-27.

11. Litynski J, Plasynski S, Spangler L, Finley R, Steadman E, Ball D et al. (2009), U.S. department of energy's regional carbon sequestration partnership program: overview, Energy Proc, 1:3959–3967.

12. Lackner KS (2003), A guide to CO_2 sequestration, Science, 300(5626):1677-1678.

13. Wood R et al. (2011), Shale gas: a provisional assessment of climate change and environmental impacts. A report commissioned by the Cooperative and undertaken by researchers at the Tyndall Centre, University of Manchester

14. Olajire AA (2011), CO_2 capture and separation technologies for end-of-pipe application – a review, Energy, 35:2610-2628.

15. Singha D, Croiseta E, Douglasa PL, Douglasb MA (2003), Techno-economic study of CO_2 capture from an existing coal-fired power plant: MEA scrubbing vs. O_2/CO_2 recycle combustion, Energy Conversion and Management, 44(19):3073-91.

16. de Visser E, Hendriks C, Barrio M, Molnvik M, Dekoeijer G, Liljemark S et al. (2008), Dynamis CO_2 quality recommendations, Int. J. Greenhouse Gas Control, 2(4):478-484.

17. Eldevik F, Graver B, Torbergsen LE, Saugerud OT (2009), Development of a Guideline for Safe, Reliable and Cost Efficient Transmission of CO_2 in Pipelines, Energy Procedia, 1(1):1579-1585.

18. Samanta A, Zhao A, Shimizu GKH, Sarkar P, Gupta R (2012), Post-Combustion CO_2 Capture Using Solid Sorbents: A Review, Ind. Eng. Chem. Res., 51(4):1438-63.

19. Choi S, Drese JH, Jones CW (2009), Adsorbent Materials for Carbon Dioxide Capture from Large Anthropogenic Point Sources, ChemSusChem, 2, 796-854.

20. Yu CH, Huang CH, Tan CS (2012), A review of CO_2 capture by Absorption and Adsorption, Aerosol and Air Quality Resaerch, 12:745-769.

21. Caplow M (1968), Kinetics of carbamate formation and breakdown, J. Am. Chem. Soc., 90 (24):6795–6803

22. Li W, Choi S, Drese JH, Hornbostel M, Krishnan G, Eisenberger PM, Jones CW (2010), Steam-stripping for regeneration of supported amine-based CO_2 adsorbents, ChemSusChem, 3(8):899-903.

23. Nakagawa K, Ohashi T (1998), A Novel Method of CO_2 Capture from High Temperature Gases, J. Electrochem. Soc., 145(4):1344-1346.

24. Hasan MM, First EL, Floudas CA (2013), Cost-effective CO_2 capture based on in silico screening of zeolites and process optimization, Phys ChemChem Phys.,15(40): 17601-18.

25. Walton KS, Abney MB, Levan MD (2006), CO_2 adsorption in Y and X zeolites modified by alkali metal cation exchange, Microporous and Mesoporous Materials, 91 (1-3):78–84.

26. Ding Y, Alpay E (2000), Equilibria and kinetics of CO_2 adsorption on hydrotalcite adsorbent, Chemical Engineering Science, 55 (17):3461–3474.

27. Siriwardane RV, Shen MS, Fisher EP (2005), Adsorption of CO_2 on Zeolites at Moderate Temperatures, Energy Fuels, 19(3):1153-1159.

28. Siriwardane RV, Shen MS, Fisher EP, Poston JA (2001), Adsorption of CO_2 on Molecular Sieves and Activated Carbon, Energy Fuels, 15 (2):279–284.

29. Kikkinides ES, Yang RT, Cho SH (1993), Concentration and recovery of carbon dioxide from flue gas by pressure swing adsorption, Ind. Eng. Chem. Res., 32 (11):2714–2720.

30. Li JR, Mab Y, McCarthyb MC, Sculleya J, Yub J, Jeong HK, Balbuena PB, Zhou HC (2011), Carbon dioxide capture-related gas adsorption and separation in metal-organic frameworks, Coordination Chemistry Reviews, 255(15–16):1791–1823.

31. Li JR, Kuppler RJ, Zhou HC (2009), Selective gas adsorption and separation in metal-organic frameworks. Chem. Soc. Rev., 38:1477-1504.

32. Davis J, Rochelle G (2009), Thermal degradation of monoethanolamine at stripper conditions, Energy Procedia, 1(1):327-333.

33. Mimura T, Simayoshi H, Suda T, Iijima M, Mituoka S (1997), Development of energy saving technology for flue gas carbon dioxide recovery in power plant by chemical absorption method and steam system, Energy Conversion and Management, 38:57-62.

34. Fytianosa G, Vevelstadb SJ, Knuutilaa HK (2016), Degradation and corrosion inhibitors for MEA-based CO_2 capture plants, Int J Greenhouse Gas Ctrl, 50:240-247.

35. DuPart MS, Bacon TR, Edwards DJ (1993), Understanding corrosion in alkanolamine gas treating plants: part 1, Hydrocarbon Process, 72(4):75–80.

36. Phan A, Doonan CJ, Uribe-Romo FJ, Knobler CB, O'Keeffe M, Yaghi OM. (2010), Synthesis, structure, and carbon dioxide capture properties of zeoliticimidazolate frameworks, AccChem Res, 43(1):58-67.

37. Adams LB, Hall CR, Holmes RJ, Newton RA (1988), An examination of how exposure to humid air can result in changes in the adsorption properties of activated carbons, Carbon, 26 (4): 451-459.

38. Verma SK, Walker PL (1992), Preparation of carbon molecular sieves by propylene pyrolysis over microporous carbons, Carbon, 30(6):829-836.

39. Riebesell U, Schulz KG, Bellerby RG, Botros M, Fritsche P, Meyerhöfer M, Neill C, Nondal G, Oschlies A, Wohlers J, Zöllner E (2007), Enhanced biological carbon consumption in a high CO_2 ocean, Nature, 450(7169):545-8.

40. Kaplan A, Reinhold L (1999), CO_2 concentrating mechanisms in photosynthetic microorganisms, Annu Rev Plant Physiol Plant Mol Biol, 50:539-570.

41. Jajesniak P, Omar A, Wong TS (2014), Carbon dioxide capture and utilization using biological systems: opportunities and challenges. J Bioprocess Biotech 4:155.

42. Channon K, Bromley EHC, Woolfson DN (2008), Synthetic biology through biomolecular design and engineering, Current Opinion in Structural Biology, 18(4):491-498.

43. Tang SY, Bourne RA, Smith RL, Poliakoff M (2008), The 24 Principles of Green Engineering and Green Chemistry: "IMPROVEMENTS PRODUCTIVELY", Green Chem, 10: 268-269.

44. Li D, Furukawa H, Deng H, Liu C, Yaghi OM, Eisenberg DS (2013), Designed amyloid fibers as materials for selective CO_2 capture, Proc Natl AcadSci, 111(1):191-6.

45. Whitesides GM, Grzybowski B (2002), Self-assembly at all scales, Science, 295(5564):2418-21.

46. Philp D, Stoddart JF (1996), Self-Assembly in Natural and Unnatural Systems, Angew. Chem. Int. Ed. Engl., 35: 1154–1196.

47. Ikkala O, Brinke GT (2002), Functional materials based on self-assembly of polymeric supramolecules, Science, 295(5564):2407-2409.

48. Knowles TP, Buehler MJ (2011), Nanomechanics of functional and pathological amyloid materials, Nat Nanotechnol., 6(8):469-79.

49. Seeman NC (2003), DNA in a material world, Nature, 421(6921):427-31.

50. Hoyer W, Cherny D, Subramaniam V, Jovin TM (2004), Rapid Self-assembly of α-Synuclein Observed by In Situ Atomic Force Microscopy, Journal of Molecular Biology, 340(1):127-139.

51. Marsh EN, DeGrado WF (2002), Noncovalent self-assembly of a heterotetrameric diiron protein, Proc Natl Acad Sci U S A, 99(8):5150-4.

52. Cadena-Nava RD, Comas-Garcia M, Garmann RF, Rao ALN, Knobler CM, Gelbart WM (2012), Self-assembly of viral capsid protein and RNA molecules of different sizes: requirement for a specific high protein/RNA mass ratio, J Virol, 86 (6):3318-3326.

53. McManus JJ, Charbonneau P, Zaccarelli E, Asherie N (2016), The physics of protein self-assembly, Current Opinion in Colloid & Interface Science, 22:73-79.

54. Wang J, Liu K, Xing R, Yan X (2016), Peptide self-assembly: thermodynamics and kinetics, ChemSoc Rev, 45:5589-5604.

55. Tsonchev S, Niece KL, Schatz GC, Ratner MA, Stupp SI (2008), Phase diagram for assembly of biologically-active peptide amphihiles, J. Phys. Chem. B, 112(2):441-447.

56. Kabiri M, Unsworth LD (2014), Application of Isothermal Titration Calorimetry for Characterizing Thermodynamic Parameters of Biomolecular Interactions: Peptide Self-Assembly and Protein Adsorption Case Studies, Biomacromolecules, 15(10):3463-3473.

57. Richardson JJ, Bjornmalm M, Caruso F (2015), Technology-driven layer-by-layer assembly of nanofilms, Science, 348(6233):aaa2491.

58. de la Rica R, Matsui H (2010), Applications of peptide and protein-based materials in bionanotechnology, Chem Soc Rev, 39(9):3499-509.

59. Smith KH, Tejeda-Montes E, Poch M, Mata A (2011), Integrating top-down and self-assembly in the fabrication of peptide and protein-based biomedical materials. Chem Soc Rev, 40(9):4563-77.

60. Zhang S (2003), Fabrication of novel biomaterials through molecular self-assembly., Nat Biotechnol., 21(10):1171-8.

61. Bong DT, Ghadiri MR (2001), Self-Assembling Cyclic Peptide Cylinders as Nuclei for Crystal Engineering, AngewChemInt Ed Engl., 40(11):2163-2166.

62. Holmes TC, de Lacalle S, Su X, Liu G, Rich A, Zhang S (2000), Extensive neurite outgrowth and active synapse formation on self-assembling peptide scaffolds., Proc Natl AcadSci U S A., 97(12):6728-33.

63. Vauthey S, Santoso S, Gong H, Watson N, Zhang S (2002), Molecular self-assembly of surfactant-like peptides to form nanotubes and nanovesicles., Proc Natl AcadSci U S A., 99(8):5355-60.

64. Ghadiri MR, Granja JR, Buehler LK (1994), Artificial transmembrane ion channels from self-assembling peptide nanotubes, Nature, 369(6478):301-4.

65. Chiti F, Dobson CM (2006), Protein misfolding, functional amyloid, and human disease., Annu Rev Biochem., 75:333-66.

66. Qiu WQ, Folstein MF (2006), Insulin, insulin-degrading enzyme and amyloid-β peptide in Alzheimer's disease: review and hypothesis, Neurobiol Aging., 27(2):190-8.

67. Reiman EM (2016), Alzheimer's disease: Attack on amyloid-β protein, Nature, 537(7618):36-7.

68. Harper JD, Lansbury PT (1997), Jr Models of amyloid seeding in Alzheimer's disease and scrapie: mechanistic truths and physiological consequences of the time-dependent solubility of amyloid proteins. Annu Rev Biochem., 66:385–407.

69. Ferrone F (1999), Analysis of protein aggregation kinetics, Methods Enzymol, 309:256-74.

70. Jarrett JT, Lansbury PT (1993), Jr Seeding "one-dimensional crystallization" of amyloid: a pathogenic mechanism in Alzheimer's disease and scrapie? Cell, 73:1055–8.

71. Xue WF, Homans SW, Radford SE (2008), Systematic analysis of nucleation-dependent polymerization reveals new insights into the mechanism of amyloid self-assembly, Proc Natl AcadSci, 105(26):8926-31.

72. Harper JD, Lansbury PT Jr (1997), Models of amyloid seeding in Alzheimer's disease and scrapie: mechanistic truths and physiological consequences of the time-dependent solubility of amyloid proteins. Annu Rev Biochem, 66:385–407.

73. Nelson R, Sawaya MR, Balbirnie M, Madsen AØ, Riekel C, Grothe R, Eisenberg D (2005), Structure of the cross-β spine of amyloid-like fibrils., Nature, 435(7043):773-8.

74. Sawaya MR, Sambashivan S, Nelson R, Ivanova MI, Sievers SA, Apostol MI, Thompson MJ, Balbirnie M, Wiltzius JJ, McFarlane HT, Madsen AØ, Riekel C,

Eisenberg D (2007), Atomic structures of amyloid cross-β spines reveal varied steric zippers, Nature, 447(7143):453-7.

75. Cannon MJ, Williams AD, Wetzel R, Myszka DG (2004), Kinetic analysis of β -amyloid fibril elongation, Anal Biochem, 328(1):67-75.

76. Glenner GG, Page DL, EANES ED (1972), The relation of the properties of congo red-stained amyloid fibrils to the β-conformation, Journal of Histochemistry & Cytochemistry, 20(10):821-826.

77. LeVine H (1999), Quantification of β -sheet amyloid fibril structures with thioflavin T., Methods Enzymol. 309:274-84.

78. Makin OS, Atkins E, Sikorski P, Johansson J, and Serpell LC (2005), Molecular basis for amyloid fibril formation and stability,Proc Natl AcadSci, 102 (2) 315-320.

79. Gazit E (2002), A possible role for pi-stacking in the self-assembly of amyloid fibrils, FASEB J, 16(1):77-83.

80 . Smith JF, Knowles TP, Dobson CM, Macphee CE, Welland ME (2006), Characterization of the nanoscale properties of individual amyloid fibrils. Proc Natl AcadSci USA,103:15806–11.

81. Meersman F, Dobson CM (2006), Probing the pressure-temperature stability of amyloid fibrils provides new insights into their molecular properties. Biochem BiophysActa., 1764:452–60.

82. Eisenberg D, Jucker M (2012), The amyloid state of proteins in human diseases. Cell, 148(6):1188-203.

83. Sunde M, Blake C (1997), The structure of amyloid fibrils by electron microscopy and X-ray diffraction. Adv Protein Chem, 50:123–59.

84. Sipe JD, Cohen AS (2000), Review: history of the amyloid fibril, J Struct Biol., 130(2-3):88-98.

85. Petkova AT, Leapman RD, Guo Z, Yau WM, Mattson MP, Tycko R (2005), Self-propagating, molecular-level polymorphism in Alzheimer's β -amyloid fibrils, Science, 307(5707):262-5.

86. Chapman MR, Robinson LS, Pinkner JS, Roth R, Heuser J, Hammar M (2002), Role of Escherichia coli curli operons in directing amyloid fiber formation. Science, 295:851–5.

87. True HL, Lindquist SL (2000), A yeast prion provides a mechanism for genetic variation and phenotypic diversity. Nature, 407:477–83.

88. Maji SK, Perrin MH, Sawaya MR, Jessberger S, Vadodaria K, Rissman RA et al. (2009), Functional amyloids as natural storage of peptide hormones in pituitary secretory granules. Science, 325:328–32.

89. Gras SL, Tickler AK, Squires AM, Devlin GL, Horton MA, Dobson CM et al. (2008), Functionalised amyloid fibrils for roles in cell adhesion. Biomaterials, 29:1553–62

90. Horii A, Wang X, Gelain F, Zhang S (2007), Biological designer self-assembling peptide nanofiber scaffolds significantly enhance osteoblast proliferation, differentiation and 3-D migration. PLoS One, 2:e190.

91. Koutsopoulos S, Unsworth LD, Nagai Y, Zhang S (2009), Controlled release of functional proteins through designer self-assembling peptide nanofiber hydrogel scaffold. Proc Natl AcadSci USA, 106:4623–8.

92. Maji SK, Schubert D, Rivier C, Lee S, Rivier JE, Riek R (2008), Amyloid as a depot for the formulation of long-acting drugs. Plos Biology, 6:e17.

93. Reches M, Gazit E (2003), Casting metal nanowires within discrete self-assembled peptide nanotubes. Science, 300:625–7.

94. Gazit E (2007), Self assembly of short aromatic peptides into amyloid fibrils and related nanostructures. Prion, 1:32–5

95. Mitraki A, Barge A, Chroboczek J, Andrieu JP, Gagnon J, Ruigrok RW (1999), Unfolding studies of human adenovirus type 2 fibre trimers. Evidence for a stable domain, Eur J Biochem, 264(2):599-606.

96. van Raaij MJ, Mitraki A, Lavigne G, Cusack S (1999), A triple β -spiral in the adenovirus fibre shaft reveals a new structural motif for a fibrous protein, Nature, 401(6756):935-8.

97. Papanikolopoulou K, Schoehn G, Forge V, Forsyth VT, Riekel C, Hernandez JF, Ruigrok RW, Mitraki A (2005), Amyloid fibril formation from sequences of a natural β -structured fibrous protein, the adenovirus fiber, J BiolChem, 280(4):2481-90.

98. Tamamis P, Kasotakis E, Mitraki A, Archontis G (2009), Amyloid-like self-assembly of peptide sequences from the adenovirus fiber shaft: insights from molecular dynamics simulations, J Phys Chem B, 113(47):15639-47.

99. Kasotakis E, Mossou E, Adler-Abramovich L, Mitchell EP, Forsyth VT, Gazit E, Mitraki A (2009), Design of metal-binding sites onto self-assembled peptide fibrils, Biopolymers, 92(3):164-72.

100. Tamamis P, Archontis G (2011), Amyloid-like self-assembly of a dodecapeptide sequence from the adenovirus fiber shaft: Perspectives from molecular dynamics simulations, J Non-Crystalline Solids, 357:717-722.

101. Tamamis P, Terzaki K, Kassinopoulos M, Mastrogiannis L, Mossou E, Forsyth VT, Mitchell EP, Mitraki A, Archontis G (2014), Self-assembly of an aspartate-rich sequence from the adenovirus fiber shaft: insights from molecular dynamics simulations and experiments, J Phys Chem B. 118(7):1765-74.

102. Kasotakis E, Mitraki A (2012), Silica biotemplating by self-assembling peptides via serine residues activated by the peptide amino terminal group, Biopolymers, 98(6):501-9.

103. Terzaki K, Kalloudi E, Mossou E, Mitchell EP, Forsyth VT, Rosseeva E, Simon P, Vamvakaki M, Chatzinikolaidou M, Mitraki A, Farsari M (2013), Mineralized self-assembled peptides on 3D laser-made scaffolds: a new route toward 'scaffold on scaffold' hard tissue engineering, Biofabrication, 5(4):045002.

104. Deidda G, Jonnalagadda SVR, Spies JW, Ranella A, Mossou E, Forsyth VT, Mitchell EP, Bowler MW, Tamamis P, Mitraki A (2016), Self-Assembled Amyloid Peptides with Arg-Gly-Asp (RGD) Motifs As Scaffolds for Tissue Engineering, ACS Biomater. Sci. Eng.

105. Tamamis P, Kasotakis E, Archontis G, Mitraki A (2014), Combination of Theoretical and Experimental Approaches for the Design and Study of Fibril-Forming Peptides, Methods in Molecular Biology, 1216:53-67.

106. Brooks BR, Brooks CL III, Mackerell AD Jr, Nilsson L, Petrella RJ, Roux B et al. (2009), CHARMM: the biomolecular simulation program, J Comput Chem 30:1545–1614.

107. Pieridou G, Avgousti-Menelaou C, Tamamis P, Archontis G, Hayes SC (2011), UV resonance, Raman study of TTR (105–115) structural evolution as a function of temperature, J Phys Chem B 115:4088–4098.

108. Swendsen R, Wang J (1987), Non-universal critical dynamics in Monte Carlo simulations, Phys Rev Lett 57:2607–2609.

109. Hukushima K, Nemoto K (1996), Exchange Monte Carlo method and application to spin glass simulation, J Phys Soc Jpn 65:1604–1608.

110. Nymeyer H, Gnanakaran S, Garcia A (2004), Atomic simulations of protein folding, using the replica exchange algorithm. Methods Enzymol 30:119–149.

111. Frishman D, Argos P (1995), Knowledge-based secondary structure assignment. Proteins, 23:566–579.

112. Kabsch W, Sander C (1983), Dictionary of protein secondary structure: pattern recognition of hydrogen-bonded and geometrical features, Biopolymers 22:2577–2637.

113. Chandrasekhar S (1992), Liquid crystals, Cambridge University Press, Cambridge

114. Cecchini M, Rao F, Seeber M, Caflisch A (2004), Replica exchange molecular dynamics simulations of amyloid peptide aggregation, J Chem Phys 121:10748–10756.

115. Seeber M, Cecchini M, Rao F, Settanni G, Caflisch A (2007) WORDOM: a program for efficient analysis of molecular dynamics simulations, Bioinformatics 23:2625–2627.

116. Görbitz CH (2007), Microporous organic materials from hydrophobic dipeptides, Chemistry, 13(4):1022-31.

117. Comotti A, Fraccarollo A, Bracco S, Beretta M, Distefano G, Cossi M, Marchese L, Riccardi C, Sozzani P (2013), Porous dipeptide crystals as selective CO_2 adsorbents: Experimental isotherms vs. grand canonical Monte Carlo simulations and MAS NMR spectroscopy, CrystEngComm, 15(8):1503-1507.

118. Li D, Furukawa H, Deng H, Liu C, Yaghi OM, Eisenberg DS (2013), Designed amyloid fibers as materials for selective CO_2 capture, Proc Natl AcadSci, 111(1):191-6.

119. Edsall JT, Wyman J (1958) Biophysical Chemistry (Academic, New York), Vol 1.

120. Mimura T, Suda T, Iwaki I, Honda A, Kumazawa H (1998), Kinetics of reaction between carbon dioxide and sterically hindered amines for carbon dioxide recovery from power plant flue gases, Chemical Engineering Communications, 170(1):245-260.

121. Li D, Jones EM, Sawaya MR, Furukawa H, Luo F, Ivanova M, Sievers SA, Wang W, Yaghi OM, Liu C, Eisenberg DS (2014) Structure-based design of functional amyloid materials, J Am Chem Soc, 136(52):18044-51.

122. Costantino HR, Griebenow K, Mishra P, Langer R, Klibanov AM (1995), Fourier-transform infrared spectroscopic investigation of protein stability in the lyophilized form, Biochim Biophys Acta, 1253(1):69-74.

123. Lee SS, Yoo JS, Moon GH, Park SW, Park DW, Oh KJ (2004), CO_2 adsorption with attrition of dry sorbents in a fluidized bed, Chem Soc Div Fuel Chem (2004) 49(1):314-315.

124. Ebner AD, Ritter JA (2009), State-of-the-art Adsorption and Membrane Separation Processes for Carbon Dioxide Production from Carbon Dioxide Emitting Industries, Separation Science and Technology, 44:6, 1273-1421.

125. Lu W, Verdegaal WM, Yu J, Balbuena PB, Jeong HK, Zhou HC (2013), Building multiple adsorption sites in porous polymer networks for carbon capture applications, Energy Environ. Sci., 2013,6, 3559-3564.

126. Samanta A, Zhao A, Shimizu GKH, Sarkar P, Gupta R (2012), Post-Combustion CO_2 Capture Using Solid Sorbents: A Review, Ind. Eng. Chem. Res., 51(4):1438-63.